Project Number: PH-RG1-ORNL

DC GLOW-DISCHARGE PLASMA GUN

A Major Qualifying Project Report:

submitted to the Faculty

of the

WORCESTER POLYTECHNIC INSTITUTE

in partial fulfillment of the requirements for the

Degree of Bachelor of Science

by

_____

Justin R. Carmichael

Date: May 20, 2007

Approved:

_____

Professor Rafael Garcia, Major Advisor

1. plasma
2. ion
3. hydrogen

Abstract

The ion source for the Spallation Neutron Source of Oak Ridge National Laboratory is required to produce a substantial amount of H^- current. To help the ion source produce this current, a DC, glow-discharge plasma gun was designed using coupled fluid dynamic, heat transfer, mechanical stress and deformation, and ion/electron trajectory simulations. In this report, the initial design, simulations results, and experimental data will be discussed.

Acknowledgements

This research was conducted at the Spallation Neutron Source (SNS) of Oak Ridge National Laboratories (ORNL), and supported by the U.S. Department of Energy (DOE). I would like to thank the DOE for the opportunity to participate in the SULI program, as well as my mentor, Dr. Robert Welton, for his guidance and motivation. I am also indebted to the help provided by engineer Danny Crisp and technician Syd Murray Jr., who gave both suggestions regarding the design of the plasma gun discussed in this report. I also appreciate the help David Manura provided with the Simion computer simulation code, and the data provided by graduate student Jerry Carr Jr. Finally, I would like to thank Professor Rafael Garcia of WPI for his help in compiling this project report.

Table of Contents

1. Introduction

1.1 Oak Ridge National Laboratory (ORNL)

ORNL was established in 1953 as a major part of the Manhattan Project. ORNL's role in the Manhattan project was to find viable methods of refining Plutonium and Uranium for use in nuclear weapons. To support this goal, a city with an enormous infrastructure was created to house the scientists and other workers. After the war ORNL's location and purpose was declassified, though Oak Ridge is still referred to as the "secret city". In the 1950s and 1960s, the objective of ORNL was still mainly nuclear energy, though other research emerged in the physical and life sciences. [(1)]

In the 1970s, after the creation of the Department of Energy (DOE), the extent of the research at ORNL was broadened immensely. Research then included a variety of energy technologies, vast research in the life sciences, as well as in the fields of chemistry, materials science, and more. [(1)] At the turn of the century ORNL became one of the largest laboratories in the nation, with research occurring in almost every field. ORNL is now the world's largest facility for materials research, with two sources of high intensity neutron beams for scattering experiments. The US effort towards the International Thermonuclear Reactor (ITER) also occurs mostly on the ORNL campus. The Center for Nanophase Materials at ORNL houses some of the world's most sensitive electron microscopes, and the supercomputers at ORNL are among the world's most powerful. [(2)]

1.2 The Spallation Neutron Source (SNS)

The SNS began conceptual development as early as 1984 with a presentation by Ralph Moon as a part of the Seitz-Eastman committee. The committee's purpose was to review future demands for materials research facilities in the United States. The presentation given by Ralph Moon suggested two new facilities. One was to become the Advanced Photon Source at Argonne National Laboratories, which was

a synchrotron based X-ray source. Another facility was suggested that would create an intense neutron flux of greater power than any existing nuclear reactor for studying a wide range of materials properties. It was well known at the time that neutron scattering can reveal information about a material that conventional techniques, such as x-ray crystallography, cannot. With a new source of intense neutrons and accompanying instrumentation, the United States could make immense progress in the field of materials science. [3]

In 1993, President Clinton urged Congress to fund the construction of the Advanced Neutron Source (ANS) at ORNL. Funding large scientific projects at that time was met with concern and objection by congress, due to the recent failure of the Superconducting Supercollider in Texas. Nonetheless, after considerable reductions, alterations, and pushing by the DOE, construction began at ORNL in 1999. A groundbreaking ceremony occurred on December 15, 1999 with then Vice President Al Gore holding the shovel. [3]

Figure 1.1 - An aerial view of the SNS in 2006. Taken from Ref. (3)

The SNS is an incredible feat of engineering. The electrical power usage alone, at 42 MW, is enough power to supply 30,000 people. The power contained in the beam alone is enough for 1,400 homes. Every beam critical component had to be fabricated to specification within 0.2 millimeter, the size of a small mite. Furthermore, the alignment of the linear accelerator (linac) had to take the curvature of the earth into consideration. Many of the technologies in use at the SNS are brand new concepts, incuding the superconducting linac. Over 600 feet of the linac uses superconducting cavity acceleration, which is chilled to about 2 degrees Kelvin using liquid helium. [4]

1.2.1 The Operation of the SNS

The SNS was designed and built by several laboratories across the US, with the final assembly and construction occurring at ORNL. The initial Ion Source was developed at Lawrence Berkeley National Laboratory (LBNL), the Linac built at Los Alamos National Laboratory (LANL), the Accumulator Ring at Brookhaven National Laboratory (BNL), and the Target systems designed by ORNL (see Figure 1.2 for a layout of the SNS). [5]

Neutron production at the SNS starts with a relatively small component called the ion source. The ion source produces a pulsed stream of negative hydrogen ions, which enter the linac and are quickly accelerated to about 90% the speed of light. While the end goal is to produce an incredibly powerful beam of protons to hit a target with – no ion source can produce this beam at once. The trick is to have an accumulator ring to store each pulse made from the ion source, and build upon this pulse until the desired power is reached. Unfortunately, this method has its own catch; adding a proton pulse to another proton pulse in a storage ring leads to space charge problems. The proton pulses, being of opposing charges, repel each other. After a sequence of pulses the storage ring would have a 'line' of

charge instead of a tight packet. If a magnetic switch is turned on to allow the particles to escape the storage ring, they would spray some angle out of the exit before the magnetic switch was aligned. This process has to be timed precisely, and it requires a dense packet of protons.

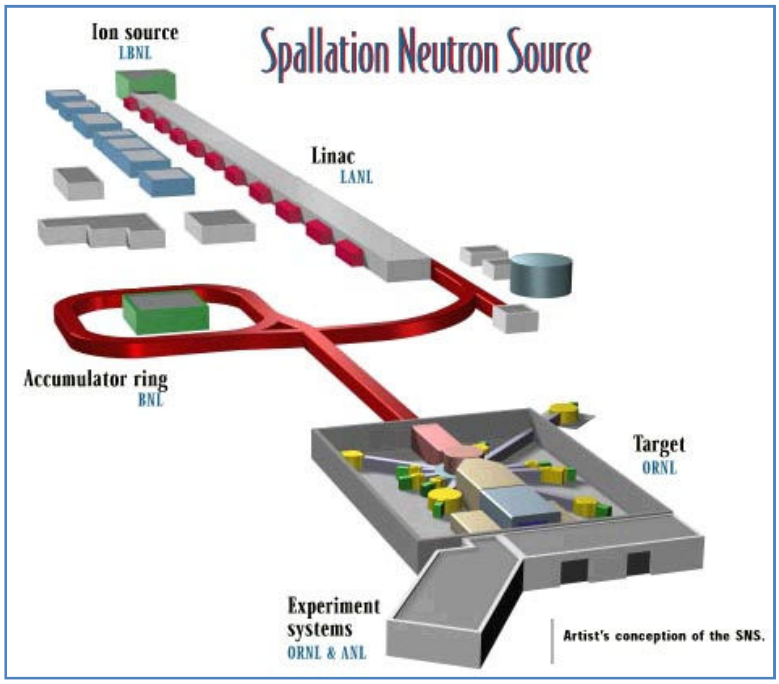

Figure 1.2 - Layout of the SNS. Taken from Ref. (5)

The way this is achieved is by using negative hydrogen ions. The H^- ions are accelerated, and before entering the storage ring are stripped of their electrons by passing through a thin foil of graphite. When the next pulse of H^- enters, it first joins with the previous proton pulse in the ring, and then passes through the foil again. This process can repeat up to approximately 1000 times before the desired power is achieved. The switching magnets are then activated, sending the proton pulse into a liquid mercury target. A tremendous flow of liquid mercury is subjected to a powerful beam of high energy protons (see Figure 1.3). These protons spallate, or rip apart, the nucleuses of the mercury atoms releasing a shower of neutrons which are then used to study materials.

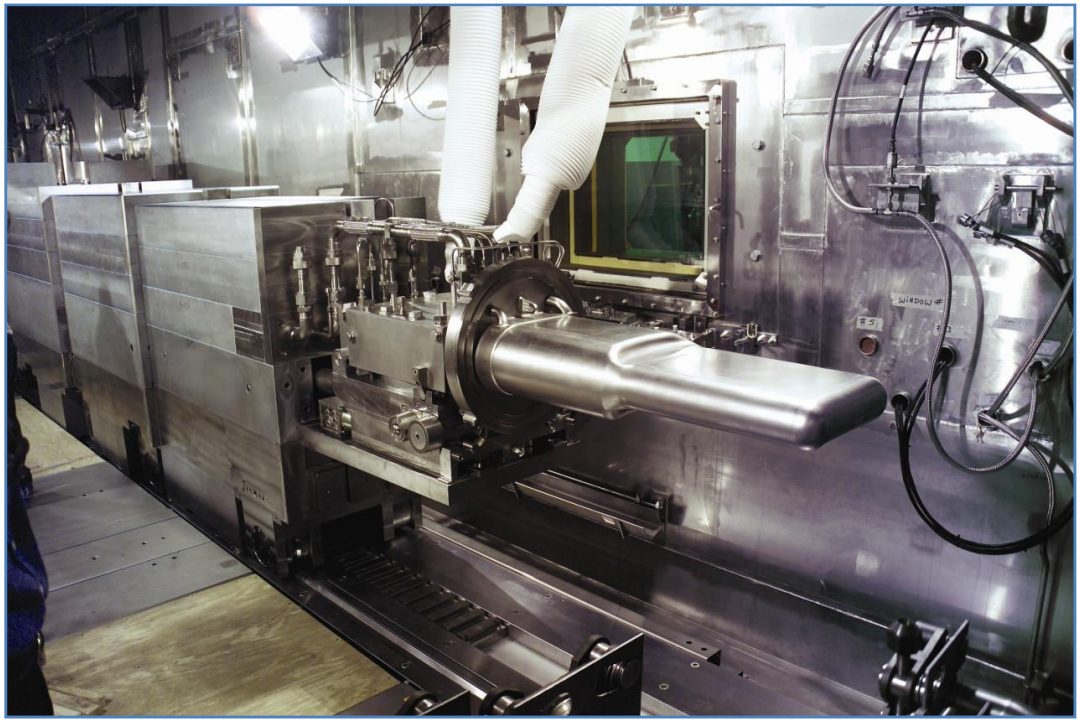

Figure 1.3 – The SNS target, in a high radiation zone, showing the robotic manipulators and leaded-glass window.

1.3 The H^- Ion Source

1.3.1 Some H^- ion source basics

For an ion source to create the H^- used by the SNS, a plasma must first be created. There are many methods of igniting and maintaining a plasma, but the design of many high current pulsed H^- ion sources relies on radio-frequency (RF) sources. In these sources, a plasma is created using an intense RF field. Electrons in a plasma are heated by the oscillating electric field of RF radiation, and these electrons increase the energy of the plasma and collide with neutral atoms to increase the ion concentration. In truly neutral plasma the number of ions, n_i, equals the number of electrons, n_e. For most ion sources at low pressures the plasma is quasineutral and there are regions of differing ion concentration.

The coupling of the RF radiation to the plasma can be treated as an electric circuit, with the plasma acting as another transformer winding. The inductance of this "coil" is the minute inertia contained from the electrons, which creates a small phase lag. There is also a characteristic resistance. The diagram is shown in Figure 1.4. [6]

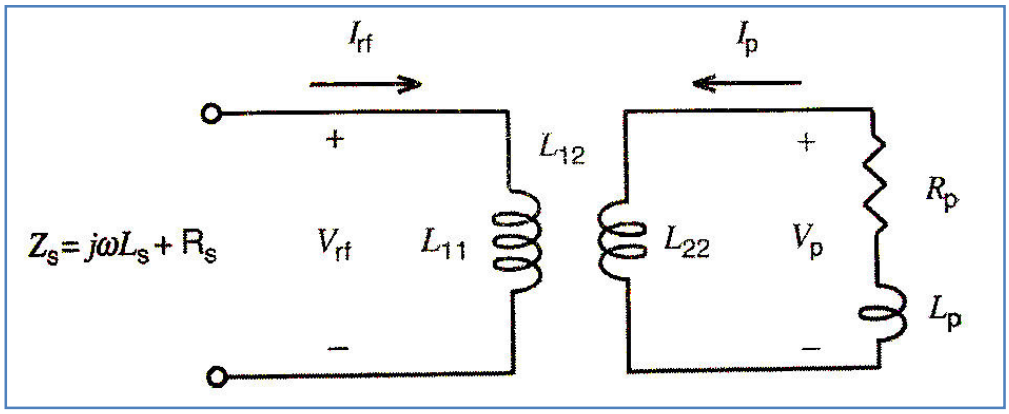

Figure 1.4 – An equivalent circuit model of the plasma discharge and RF antenna. Taken from Ref. (6)

The inductance and resistance terms of this model can be found by analyzing various plasma parameters. The plasma inductance L_s is found to be,

$$\mathbf{L_s \approx \frac{\mu_0 \pi R^2 \mathcal{N}^2}{l}\left(\frac{b^2}{R^2} - 1\right)} \qquad \textbf{(1)}$$

where 'b' is the coil radius (antenna), and 'R' is the distance from the antenna to the plasma sheath, across the dielectric barrier (ceramic wall). In this case, b-R is the dielectric gap, or in our model the distance between the two "coils". '$\mathcal{N}$' is the number of turns in the antenna, and 'l' is the length of the coil. The resistance of the plasma in the model is found by a similar means to be,

$$\boldsymbol{R_s \approx \mathcal{N}^2 \frac{\pi R}{\sigma_{eff} l \delta_p}} \qquad \textbf{(1)}$$

where σ_{eff} is the effective RF electrical conductivity, and δ_p is the collisionless skin depth of the plasma. After these are determined, it is possible to determine the required antenna current and voltage through the following relations,

$$\mathbf{P_{abs} = \frac{1}{2}|\tilde{I}_{rf}|^2 R_s} \quad \textbf{(2)}$$

where P_{abs} is the power absorbed by the plasma and $\tilde{I}_{rf}$ is the current in the antenna. The antenna voltage relation is,

$$\mathbf{\tilde{V}_{rf} = \tilde{I}_{rf}|Z_s|} \quad \textbf{(3)}$$

Calculating these parameters can help in optimizing performance, but also in the design of a suitable matching network which is required to operate the antenna. [6]

Once a plasma is created, it is often advantageous to shield it from interaction with the chamber using magnetic fields. These fields can also help improve plasma uniformity, and confine hot electrons. A multicusp magnetic confinement scheme is shown in Figure 1.5. [6]

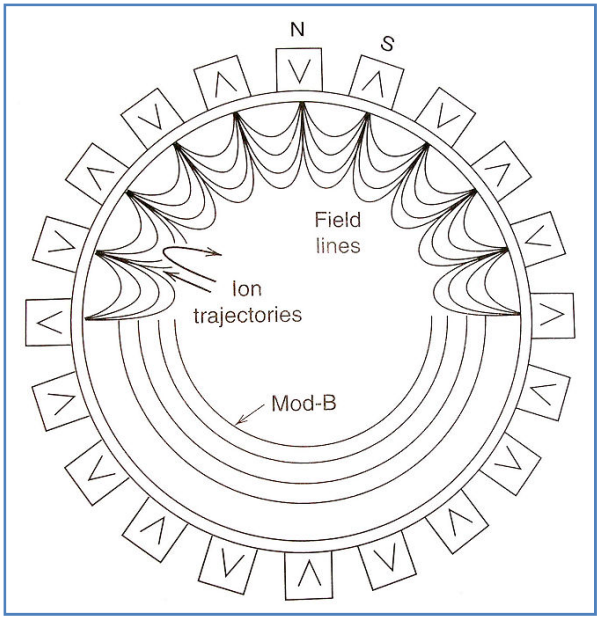

Figure 1.5 – Multicusp magnetic confinement. Taken from Ref. (6)

Inside the plasma various species of ions are created and destroyed by varied collision. This volume production can yield H^- ions, but the extra electron is weakly bounded and another energetic collision with an electron will destroy the ion. To generate more H^- ions, surface production is used which utilizes cesium. A magnetic filter field prevents energetic electrons from entering a region of the source before the aperture. Here a collar is cesiated, or deposited with a layer of cesium. Ions that come into contact with the cesium layer will undergo charge exchange, and leave the surface with a high probability of becoming H^- ions. Cesiation can increase the number of H^- ions by about a factor of three, while also reducing the number of electrons in the extracted beam by about an order of magnitude. Care has to be taken to maintain the collar temperature at about 280°C to prevent the cesium from evaporating or reacting with other elements. [7]

1.3.2 The baseline source

The baseline (presently operating on the accelerator) Ion Source at the SNS, which was used since its initial installment, is the LBNL ion source. This ion source was developed and optimized at LBNL for years,

and in 1994 it was selected by an international workshop as the most suitable ion source for the SNS. [8] The source is an internal antenna, radio frequency (RF), cesiated ion source. This means the plasma in the center of the source is ignited using pulsed RF power coupling (2 MHz, 20-60 kW), and sustained using approximately 200 W of 13.56 MHz power to the same antenna (as seen in Figure 1.6). Twenty samarium-cobalt multicusp magnets generate a magnetic field configuration which helps to contain the plasma. H^- ions are created when various ion species and neutral particles from the plasma come into contact with a cesiated surface. The LBNL source used a collar with Cs_2CrO_4 dispensers as a supply of cesium .

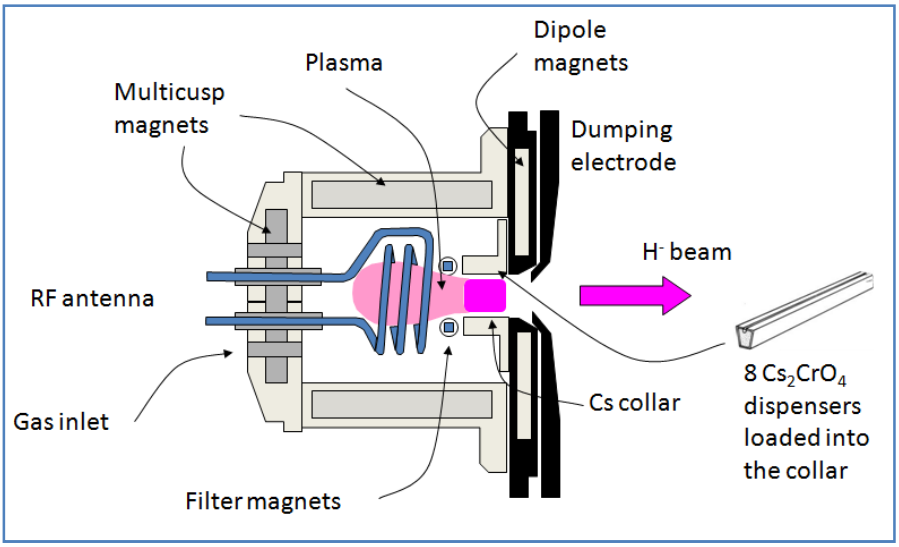

Figure 1.6 - The baseline ion source at LBNL which we are currently working towards replacing with an improved ion source based on an external antenna. Taken from Ref. (8)

The LBNL ion source worked very well during the initial SNS power runs. At a low duty-factor (a low pulse rate), the lifetime is several months of operation. The SNS, however, requires substantially higher H^- ion currents at an increased duty factor (see Figure 1.7), which severely limits the lifetime of the LBNL source. [8]

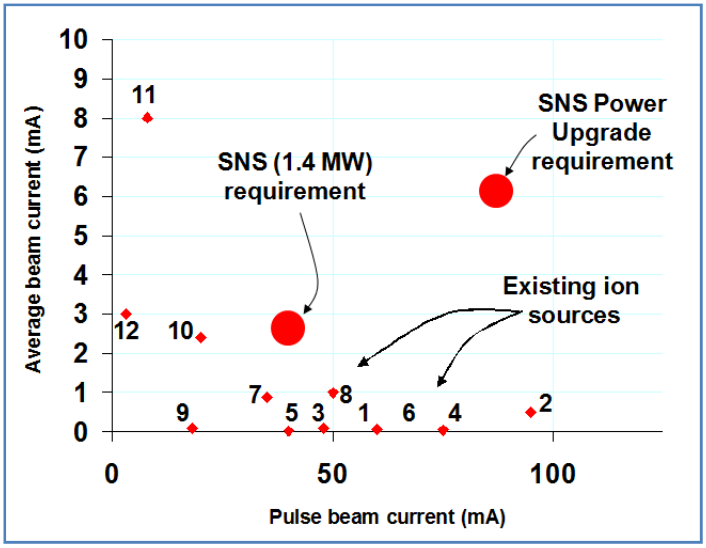

Figure 1.7 – SNS Ion Source requirements, and existing sources. The pulse beam current is the maximum current injected with a given pulse. The average beam current takes the average over time, disregarding the maximum current achieved during a pulse. Ion sources are generally made to achieve one of these objectives, as can be seen on the graph. Taken from Ref. (8)

1.3.3 Experimental H- Ion Sources at the SNS

In order to reach these demanding requirements, major design revisions have been made. To improve the lifetime the antenna was placed outside of a ceramic (Alumina, Al_2O_3) plasma chamber, which creates some power losses but drastically increases the lifetime of the source by shielding the components from the plasma. The experimental sources all have a modular design which allows for switching of various parts to test different configurations. A multicusp confinement system was designed which fits over the ceramic plasma chamber, and this can be removed or modified with ease. The cesium delivery system was modified to come from a reservoir of elemental cesium which deposits on an air cooled cesium deposition collar. By modifying the air flow the temperature of the collar can be controlled, which allows for the control of the cesium layer thickness. See Figure 1.8 for a cross sectional view of one experimental ion source.

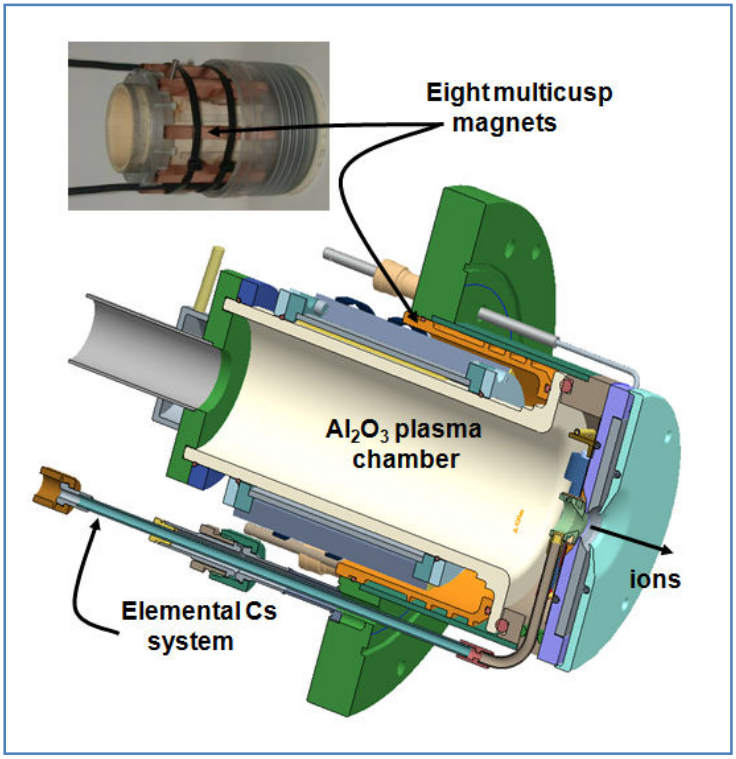

Figure 1.8 - Cross sectional view of an experimental H- ion source, showing the external antenna configuration with the modified cesium system and multicusp confinement. Reproduced with permission from Robert Welton (Ref. (9)).

1.4 Glow Discharge Plasma Sources

It was found experimentally that adding supplemental ions and electrons to the ion source plasma can greatly enhance performance. These ions and particles are created using a plasma source (or plasma gun), and preferably one with a lifetime greater than that of the ion source. One such plasma gun is the glow discharge plasma gun, which uses the effect of Paschen breakdown to ignite a plasma between a cathode and anode. Paschen breakdown occurs when two electrodes, held at some distance apart, ignite the gas between them at some specific pressure. Figure 1.9 shows one such characteristic curve for Argon. [(10)]

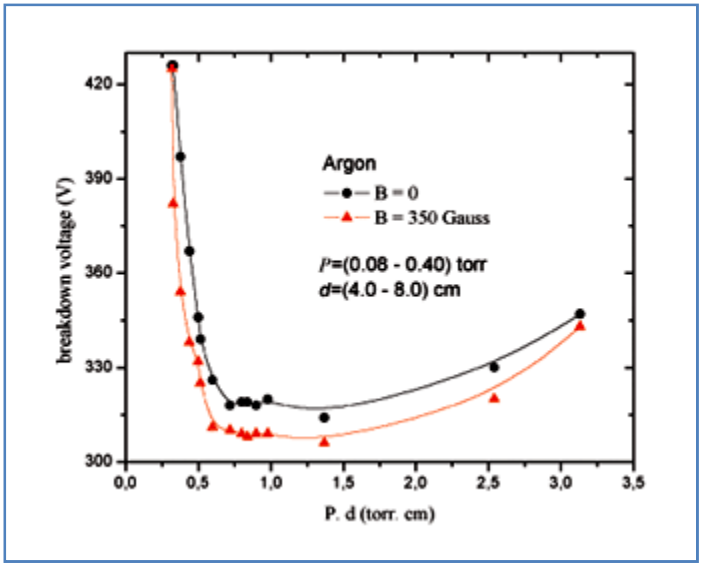

Figure 1.9 - A Paschen curve for Argon at two magnetic field strengths. The breakdown voltage is given as a function of Pd (pressure and distance). Taken from Ref. (10).

Normally this discharge does not lead to any flow in the plasma, but a static discharge. However, if a hole is created in the anode and an insulator placed between the cathode and anode which "funnels" the electric field into this aperture, plasma will be forced to exit the discharge region (see Figure 1.10). Glow discharge plasma guns operate off this simple principle, which can be improved by optimizing the geometries of the aperture, anode, cathode, and insulator.

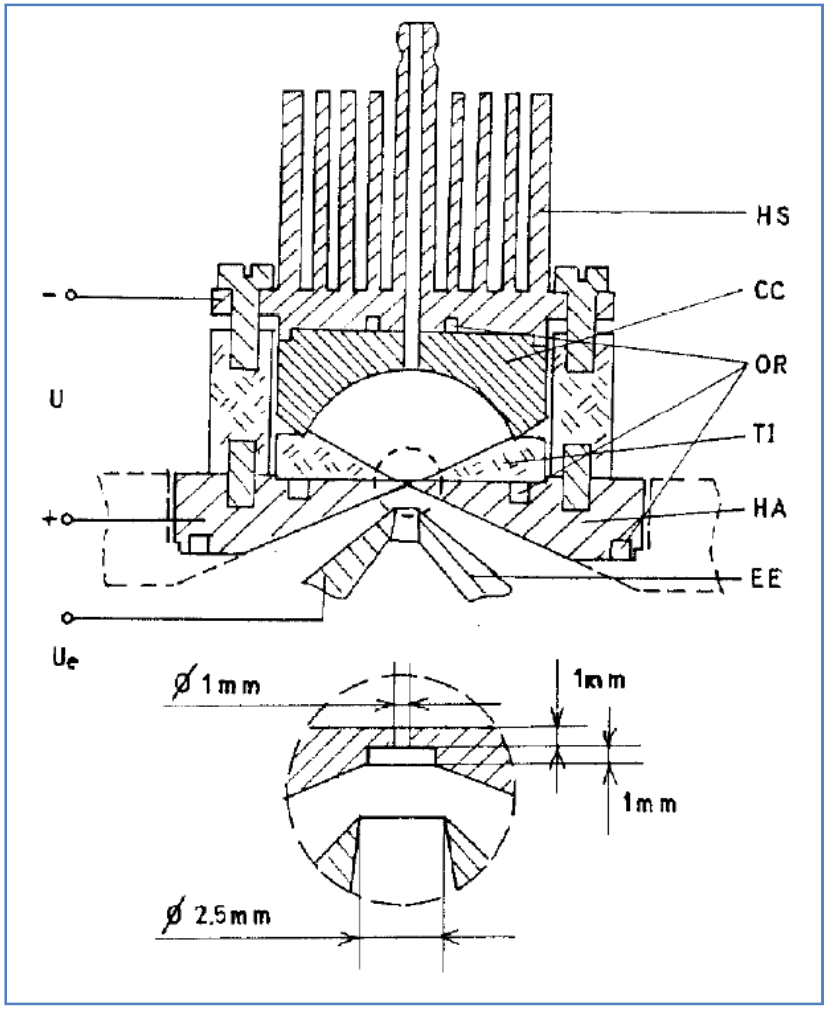

Figure 1.10 - The glow discharge (constricted aperture) plasma gun by V.I. Miljevi (Taken from Ref. (11)). The cross sectional view of the source has the various components labeled: HS – Heat Sink, CC – Concave Cathode, OR – O-Rings, TI – Teflon Insulator, HA – Hollow Anode, EE – Extraction Electrode, and the potentials U – discharge voltage, U_e – extraction voltage.

Additionally, the gas feed can be varied, and magnetic fields added to increase the emitted ion current. If a magnetic field is created axially by using a solenoid or ring magnet, the emitted ion current can increase substantially. This dependence of the magnetic field on the ion current is nonlinear, as shown in Figure 1.11.

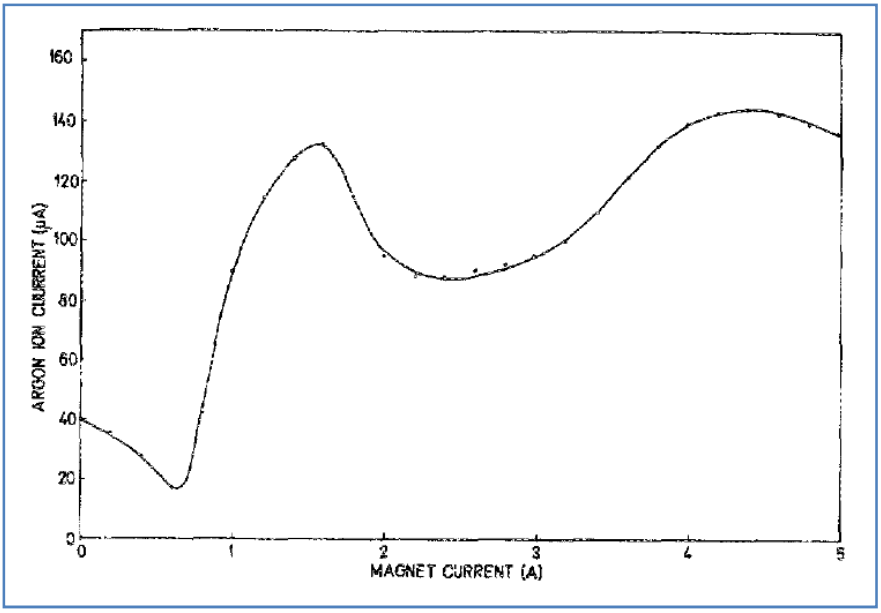

Figure 1.11 - The effect of axial magnetic field on the emitted ion current for an argon glow discharge plasma gun. The operating pressure was 0.3 torr, the discharge current was 10 mA, discharge voltage 400 V, and the extraction voltage 10 kV. Taken from Ref. (12).

The glow discharge plasma gun releases a constant flow of plasma which is useful for materials processing, or in our case, igniting an ion source. Figure 1.12 shows one such plasma gun in operation.

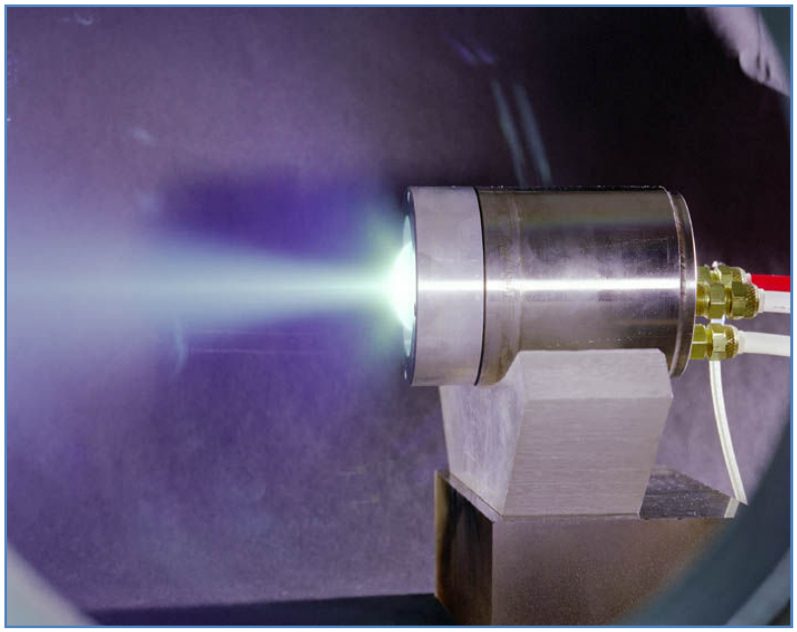

Figure 1.12 - A glow discharge plasma gun in operation on a test stand in vacuum. The plasma plume is visible, and the gas and water cooling feeds can be seen attached to the back of the source. Taken from Ref. (13).

1.4.1 The Prototype Hemispherical Plasma Gun

A prototype DC glow-discharge plasma gun was developed for use on experimental H- ion sources at the SNS (see Figure 1.13). The plasma gun consisted of a hemispherical cathode for focusing ions onto the anode aperture more effectively, and was actively water cooled. This plasma gun could produce approximately 2 mA of ion current, and did not have ion extraction capabilities.

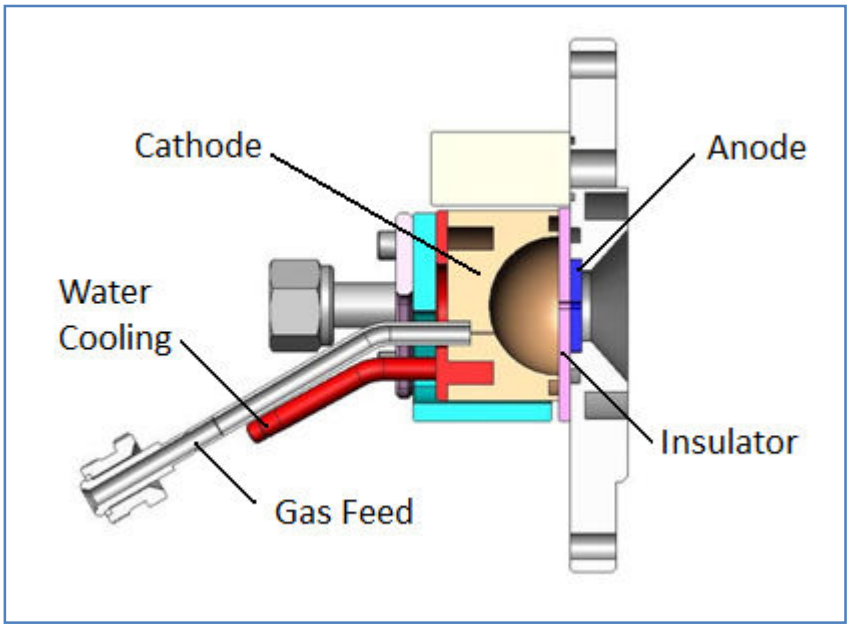

Figure 1.13 - The prototype hemispherical plasma gun for the SNS H- Ion source. The hemispherical cathode (copper) helps to focus ions towards the anode. The plasma gun is built on the back flange which attaches to the ion source. Reused with permission from the author, Robert Welton.

The size of the gun is somewhat limited because it has to be designed around the ion source back flange – which makes additional components somewhat troublesome. Adding on extraction electrodes or solenoids increases the size of the plasma gun to the extent it may no longer be compatible with the back flange. Nonetheless, the plasma gun has shown enough of an improvement to ion source performance to justify designing a more capable and powerful plasma source.

2. Mechanical Design of the Plasma Gun

2.1 Design Criteria

The SNS ion source has a 1.5 inch diameter stainless steel tube on the back flange (on the end of the ion source away from the beam). The back flange provides sealing for the ceramic chamber, some cooling, and ports for diagnostic equipment. For this reason, the completed plasma gun must be designed around the back flange such that it inserts into the 1.5 inch tube while at the same time providing an adequate vacuum seal.

The plasma gun itself must be capable of operation at 1 kW of power (1 Amp at 1 kV on the cathode), and also have an extraction electrode built in. This means the plasma gun will have three distinct regions which are held at different potentials, which would require High Voltage (HV) design with high vacuum compatibility. The cathode at 1 kW of power will require cooling to prevent melting, which means a cooling loop would have to be designed in the cathode.

Lastly, we wanted to design the gun economically, using available, non-custom, part whenever possible. Modularity of the plasma gun would also allow for switching of components in the future for different design iterations and experiments.

2.2 Initial Design Concepts

Several sketches of possible plasma gun designs were created and analyzed. The first design, shown in Figure 2.1, shows a plasma gun with all the design criteria satisfied, but is not very modular and every part is custom made, adding to the expense.

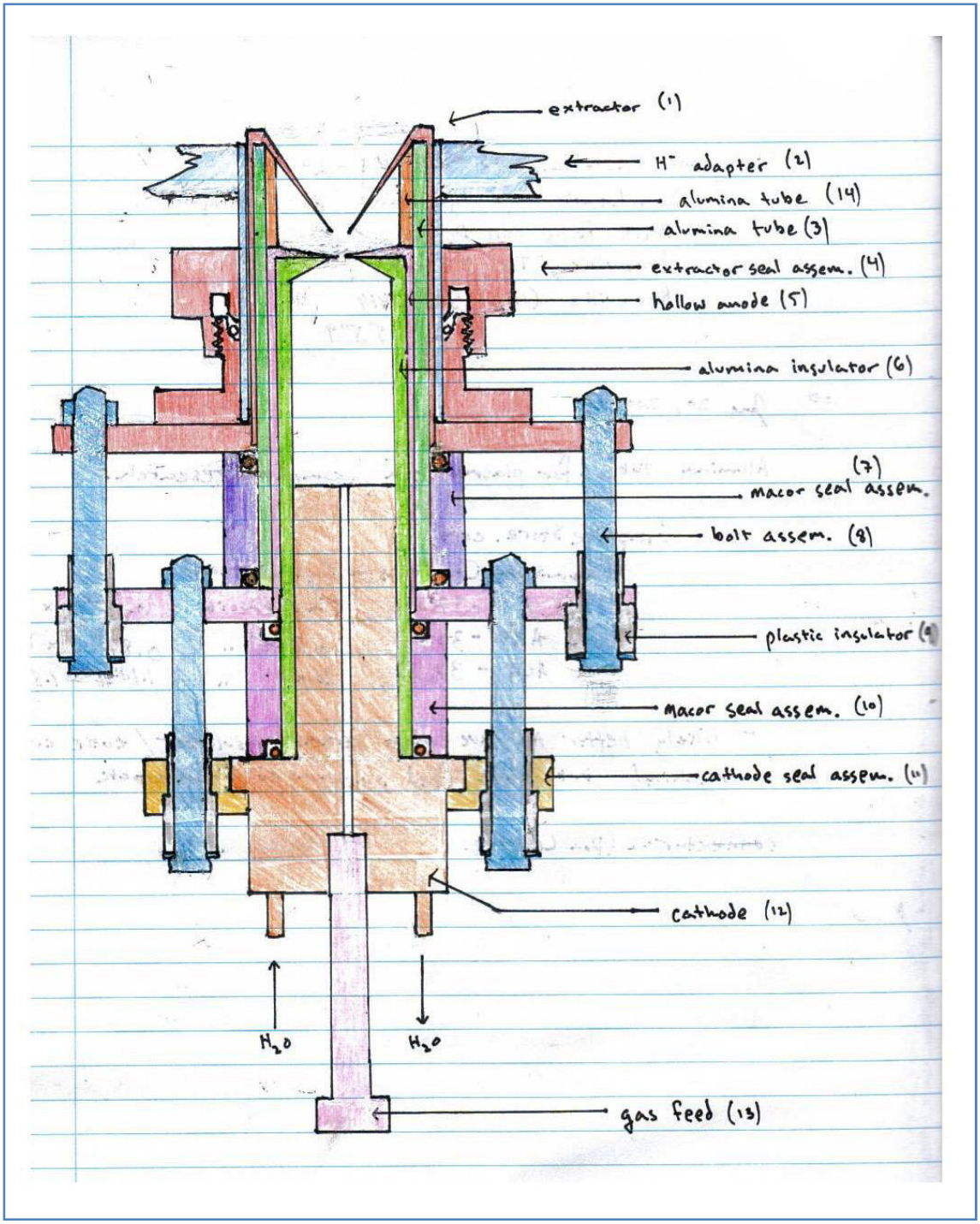

Figure 2.1 - The first design concept, showing an extractor (1), insulated using custom machined alumina parts (2, 3, 6).

The general idea was to have the components slide together and sealed using viton o-rings, with the sealing pressure provided by the bolts (shown in blue in the Figure). We decided to move forward by

using less machined ceramics, which increase the cost to a much higher extent than other customized parts. The next design, shown in Figure 2.2, uses much less ceramic components, and provides the o-ring compression using an end cap – a less complicated design than the bolted assembly.

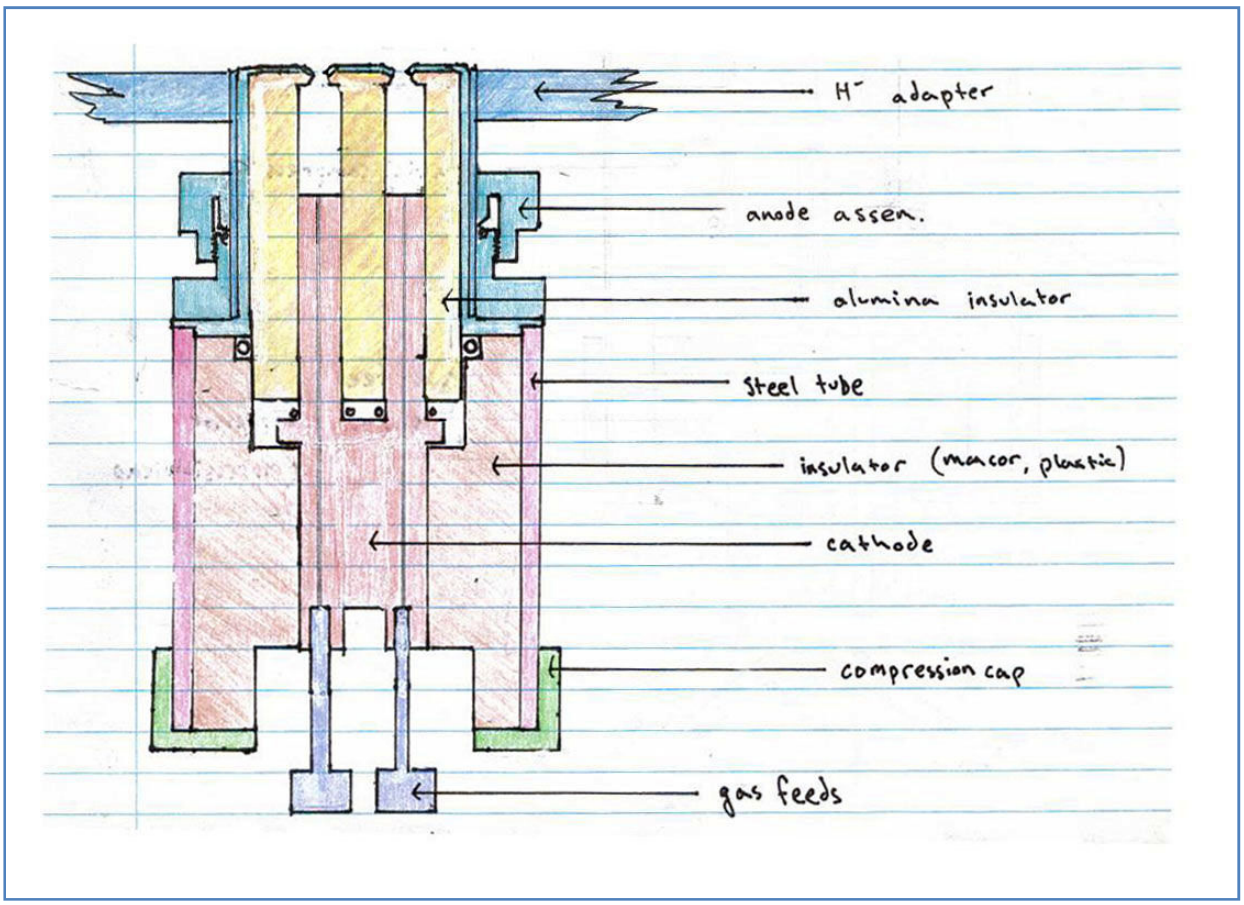

Figure 2.2 - The second design concept, greatly simplified, but lacking an extraction electrode.

This design, although an improvement, does not have an extraction electrode. The next design concept, shown in Figure 2.3, extends this design by including an extraction electrode, but the complexity increases to that of the first design. The advantage of this design is the increased modularity and compact design.

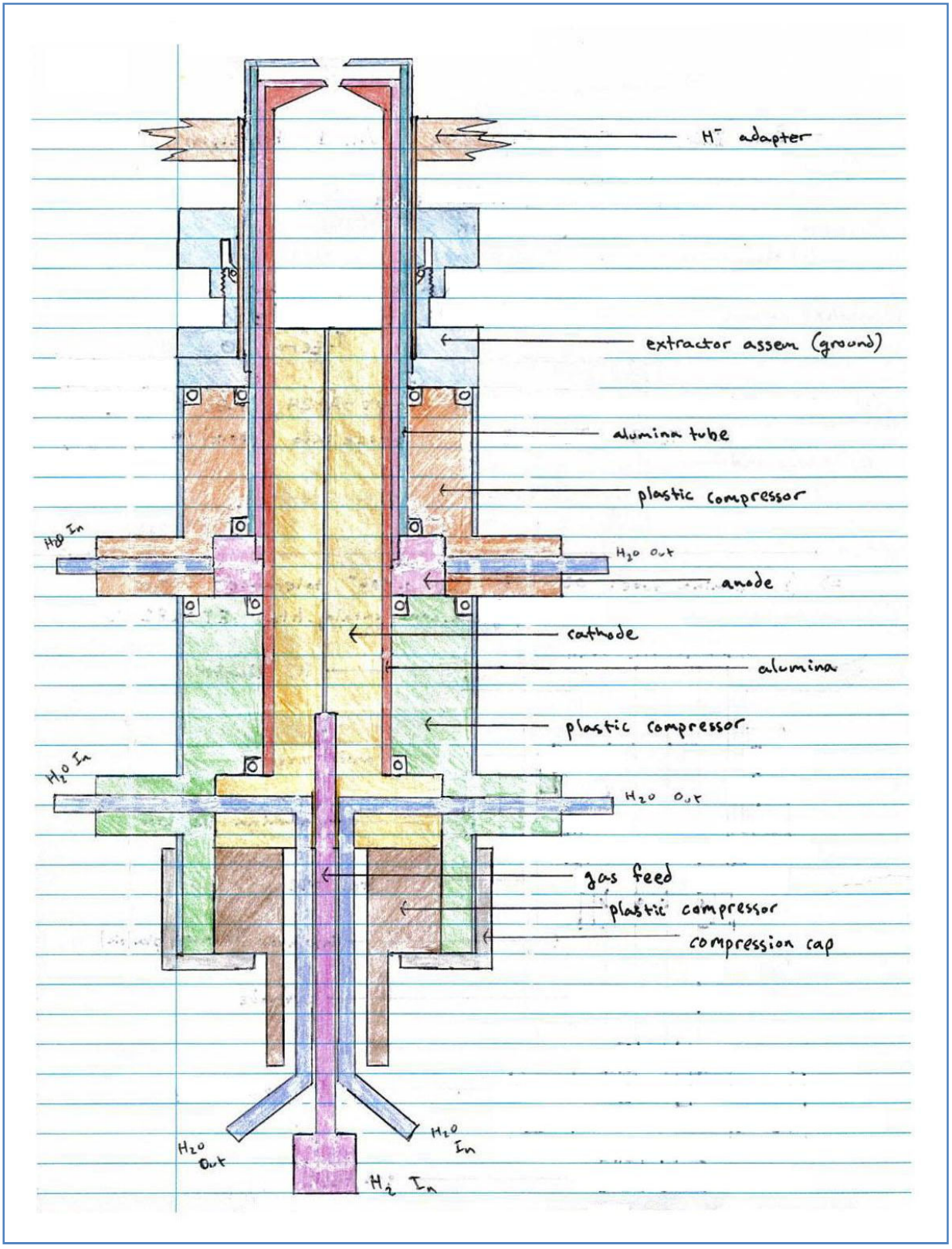

Figure 2.3 - The third design iteration, which uses the compression cap design while including an extractor electrode.

The first three designs appeared to have unavoidable complexity associated with the three separate regions. In order to design for high voltage potentials, the electrodes and attached metal components must be sufficiently insulated with plastic or ceramic. However, high vacuum design necessitates that all components in contact with the vacuum must not be made out of plastic, which generally outgases and harms the vacuum. This means that ceramics must be used to insulate the separate components, and sealed using viton o-rings. The last design concept, shown in Figure 2.4, uses the viton o-ring seals as both vacuum and high voltage insulators, greatly reducing the complexity of the plasma gun. The risk of this design is of course that one failure (either vacuum failure or high voltage breakdown) has the potential to lead to another failure.

2.3 Refinement of the Final Design

The fourth design was the design we choose to move forward with, by beginning to search for available parts and model the gun in CAD software (Solidworks). The first problem we found was that the viton o-rings are not created in standard sizes in the range required for the plasma gun. Custom sized o-rings would add to the expense, so the decision was made to use custom cut viton gaskets. The custom plastic insulator with the water coolant feeds would also be expensive to manufacture, and is generally incompatible with the cap seal design. For this reason, we modified the design to include a circular arrangement of bolts like in the first design concept.

The alumina tube insulators were found to be available, but only in a few sizes relevant to the plasma gun. These tubes were designed for use as crucibles, and are available in both closed and open end forms. The anode insulator between the cathode and anode could be created using a closed end alumina tube. Since these tubes were designed for use as crucibles, the manufactured tolerances were

large. The cathode and anode tubes that fit in or around the alumina insulators would have to be designed around the alumina tubes, and not vice versa.

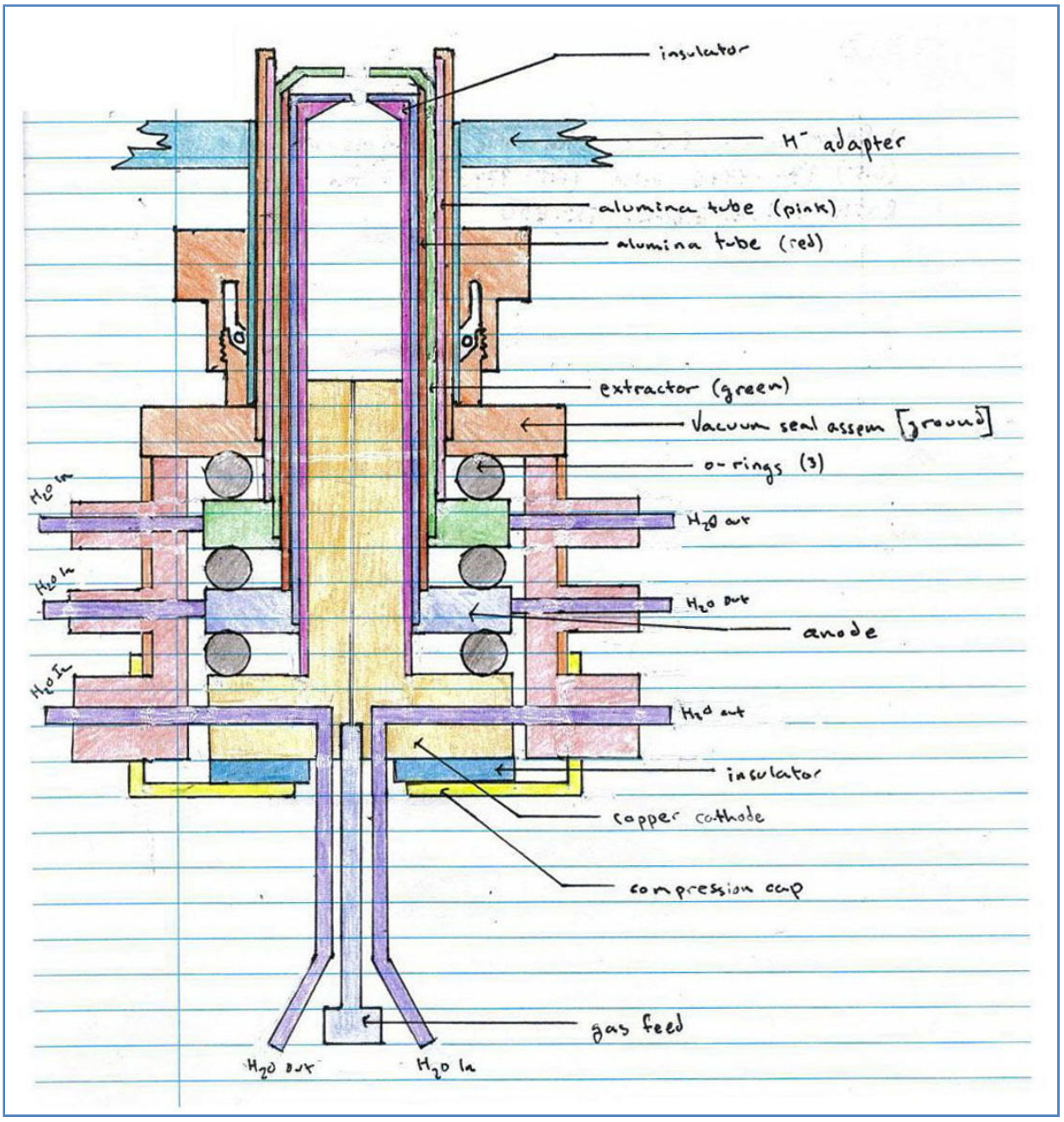

Figure 2.4 - The final design concept, showing the combined high voltage, high vacuum, viton o-ring insulators.

The cathode, anode, and extractor electrode are all insulated by these loosely tolerance alumina tubes, as shown in Figure 2.5. The cathode outer diameter (OD) had to be specified such that at elevated temperatures, the thermal expansion would not go into the alumina tube at the lowest tolerance.

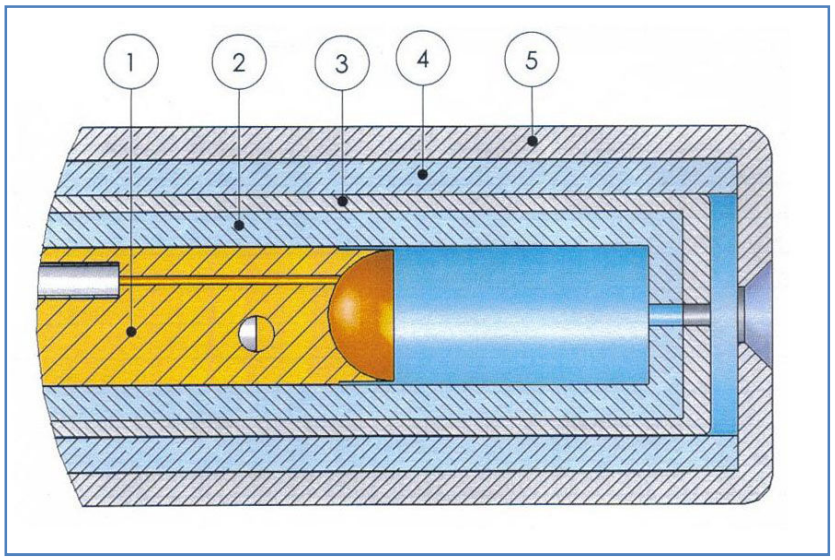

Figure 2.5 - A section view of the front of the plasma gun, showing the cathode (1), anode (3), and extractor electrode (5). These electrodes are separated by two alumina tubes (2 and 4).

If these tolerance specifications were met, the cathode OD would be too small for cooling channels and would be too loose inside the anode insulator. For this reason the exact tolerance was kept on the alumina tube with the expectation the tube may need to be modified by material removal on arrival.

The cathode itself was to be designed using a material with high thermal conductivity which can also survive ion bombardment. Copper has a high thermal conductivity, while the refractory metals (tungsten, tantalum) have the lowest sputter rates and therefore survive longer under ion bombardment. The original plan was to use tantalum or tungsten coated copper, but a bare copper electrode was used in the design to reduce the expense. This may be modified at a later time if it is found that the cathode life needs to be extended.

The cathode cooling channels were formed by machining holes along the length of the cathode and connecting them perpendicularly (see Appendix A for a set of relevant engineering drawings). This allows for laminar flow until the water changes direction in the brazed connection, which creates turbulent flow on the surface where the heat needs to be removed. Another channel was machined on the cathode for a gas feed line. This channel reduces to a much smaller diameter before entering the discharge area, to prevent the Paschen discharge from igniting the gas feed line.

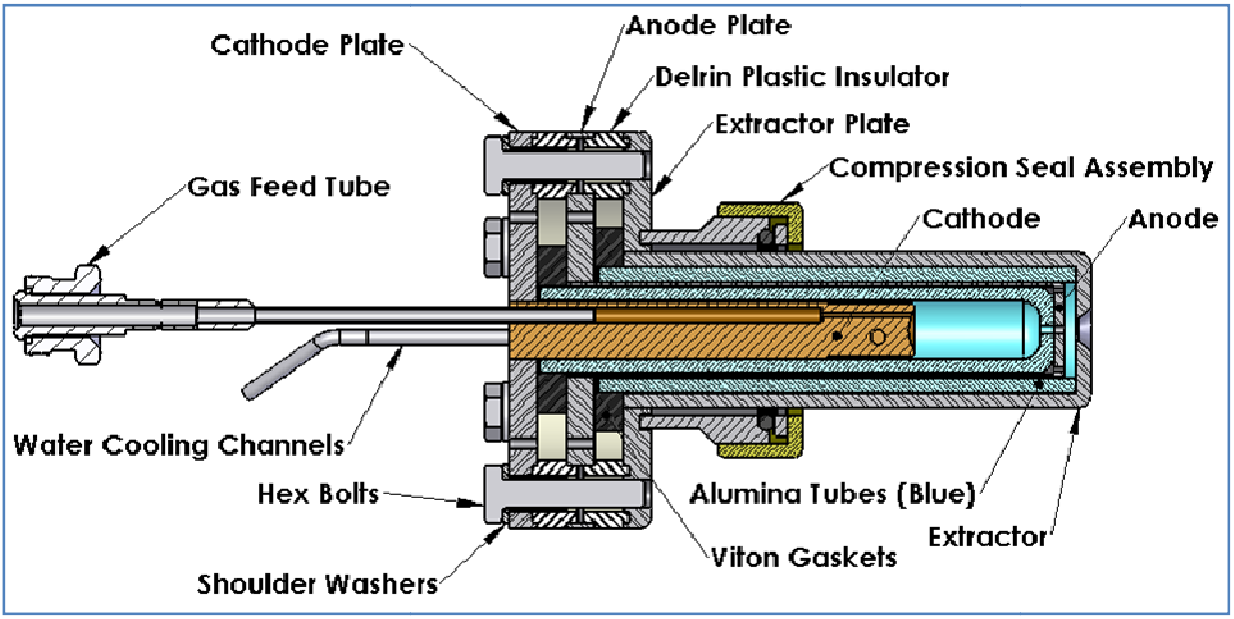

Figure 2.6 - A section view of the completed CAD model.

A complete model of the plasma gun is shown in Figure 2.6, with the components labeled. Although the mechanical design is finished with all the parts found and modeled, it is unknown if the gun can survive at 1 kW of power, or how the ions will be extracted from the given electrode.

3. Computational Fluid Dynamics and Heat Transfer Simulations

The plasma gun operates off a glow discharge plasma. This plasma is created by a DC potential between the cathode and anode. If the potential is great enough, then an ion generated will accelerate into the cathode and release a shower of secondary electrons. Particles accelerate both to the anode and to the cathode, but with the ions being the more massive particles, the cathode receives nearly all the energy. With a 1 Amp, 1 kV supply, the cathode can be exposed to nearly 1 kW of heating on its plasma facing surface. If this face were to be left uncooled, the cathode would melt resulting in a failure of the plasma gun.

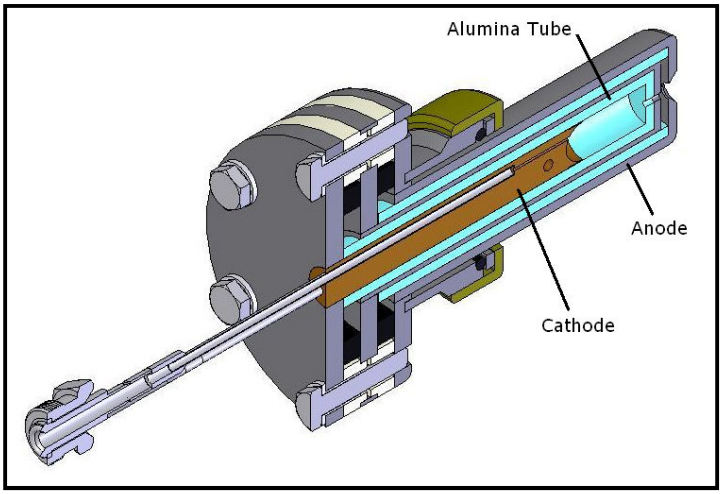

Figure 3.1 - A cross-sectional view of the plasma gun, showing the cathode, anode, and alumina tube.

The cathode's placement in the gun is shown in Figure 3.1. The face of the cathode that faces the aperture in the anode is subjected to the particle bombardment. This face must be water cooled throughout operation.

When ions hit this face they produce electrons, a process referred to as secondary electron emission. These electrons help to increase the plasma density and increase power and efficiency. For this reason, it is desirable to have a cathode face with a large surface area, provided the geometry of the cathode can still handle the designated 1 kW heat load. Creating a "jagged" surface on the cathode face would create a large surface area, but also limit the available cooling.

The cathode itself has a very small cross-sectional area in comparison to its length. Water cooling has to be transported from the back face of the plasma gun to the front face along this length. The cross-sectional area limits the water line feeds to $1/8^{th}$ inch tubes.

Considering the effects of both the surface area and the cooling loop, the design of an optimized and operable cathode becomes somewhat difficult. There is no way to analytically determine whether or not a given flow of water in a cooling loop is enough to cool the cathode face of a given geometry. The only way to ensure the cooling of the cathode face is to use coupled computational fluid dynamic (CFD) and heat transfer simulations. These numerical methods would give very good estimates as to whether or not a cathode will survive a given heat load.

The CFD simulations all solve the Navier-Stokes equations using one method or another. The general Navier-Stokes equation is

$$\boldsymbol{\rho}\left(\frac{\partial \boldsymbol{v}}{\partial \boldsymbol{t}} + (\boldsymbol{v}\cdot\boldsymbol{\nabla})\boldsymbol{v}\right) = -\boldsymbol{\nabla p} + \boldsymbol{\nabla}\cdot\mathbb{T} + \boldsymbol{f} \tag{4}$$

This equation can simplify a bit by assuming a Newtonian fluid (one which has a linear stress and strain curve, such as water), and an incompressible fluid. Though all fluids and solids are compressible to a degree, this is usually negligible in many solids. With these assumptions, the Navier-Stokes equation simplifies to

$$\boldsymbol{\rho}\left(\frac{\partial \boldsymbol{v}}{\partial \boldsymbol{t}} + (\boldsymbol{v}\cdot\boldsymbol{\nabla})\right) = -\boldsymbol{\nabla p} + \boldsymbol{\mu}\boldsymbol{\nabla}^{\mathbf{2}}\mathbf{v} + \mathbf{f} \tag{5}$$

In this equation, $\rho\left(\frac{\partial \boldsymbol{v}}{\partial t} + (\boldsymbol{v}\cdot\boldsymbol{\nabla})\boldsymbol{v}\right)$ refers to 'inertia', where $\frac{\partial \boldsymbol{v}}{\partial t}$ is the unsteady acceleration (a local acceleration), and $(\boldsymbol{v}\cdot\boldsymbol{\nabla})$ is the convective acceleration (due to the change of velocity with respect to position – such as the bulk drift in a pipe or nozzle). The $-\nabla p$ term refers to the pressure gradient, $\mu\nabla^2\mathbf{v}$ to viscosity, and 'f' to all other external forces (such as gravity or centrifugal force.

Even for extremely simple problems, the complexity behind a calculation can be overwhelming. CFD, for this reason, often is undertaken by the Finite Element Method (FEM). FEM essentially takes a large problem and breaks it down into many small, solvable, problems by employing a mesh. A mesh is a "3D grid" of elements, with each element being a "solving point" where a calculation takes place. Figure 3.2 shows a 3D object with a mesh, prior to calculation.

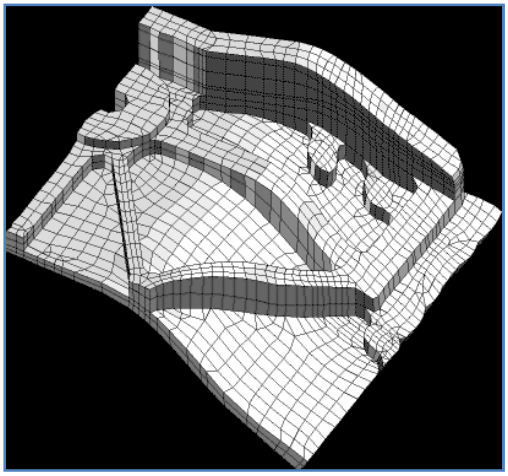

Figure 3.2 - A 3D part showing a simple mesh used in an FEM calculation. Taken from Ref. (14)

Meshing is very important with complex features, and especially when doing CFD. If a mesh is too large it will fail to capture small phenomenon, such as a narrow channel or a small vortex. In any given CFD simulation there are generally three kinds of basic mesh cells. There are fluid cells (just in the fluid flow region), solid cells (just within the solid bodies), and partial cells (between the two, on the boundary). There have to be an adequate number of cells in the fluid region or some behavior in the fluid may be incorrectly modeled. The number of partial cells must likewise be large enough to correctly show the transfer of heat from a solid body. A mesh must take all this into account, and also optimize it so that the mesh concentration is larger near areas of activity, such as a heat source or an area of turbulence in a cooling loop. A meshing algorithm can be quite complex and the meshing process can take considerable time, even when compared to the CFD calculation.

The initial design of the plasma gun was evaluated using CFD. Before fabricating the gun we wanted to have a good idea of whether or not the gun would survive, saving money and preventing downtime in the future. This would be done by first using CFD combined with heat transfer simulations, then

importing the resulting thermal distributions into another software code to determine the thermal stresses – ultimately deciding whether or not the materials used in the gun can survive the heat load from the plasma. The software we used for CFD was Cosmos FloWorks, designed for use with SolidWorks CAD software. [15]

The first design of the cathode and the plasma gun is shown in Figure 3.3. Not shown in the Figure are two 1/8 inch water lines which are drilled through the length of the copper cathode. A hole is drilled perpendicular to these two lines, connecting them. Two copper plugs are then brazed into this connecting hole to create one sealed loop, with the turbulent area at the end directly above the heated cathode face. An additional hole is drilled for the gas feed, which appears on the simulation as a hole that abruptly stops, although in reality another hole with a smaller diameter connects this hole to the cathode face. The cathode face itself is slightly hemispherical, allowing for some increased surface area and possibly some additional focusing of ions and particles towards the anode aperture.

The results of the first simulation were promising, although the temperatures were too close to the failure point of the cathode. Although the melting point of copper is about 1084°C, its vapor pressure occurs at a reduced temperature in a vacuum. Assuming the ion source's lowest pressure is on the order of 1×10^{-8} Torr, the temperature at which the evaporation occurs in Copper is about 700°C (see Appendix B). The maximum temperature found in the simulation was about 544°C. This should not cause problems, but lowering the temperature further would allow for a longer cathode life and higher operable power. [16]

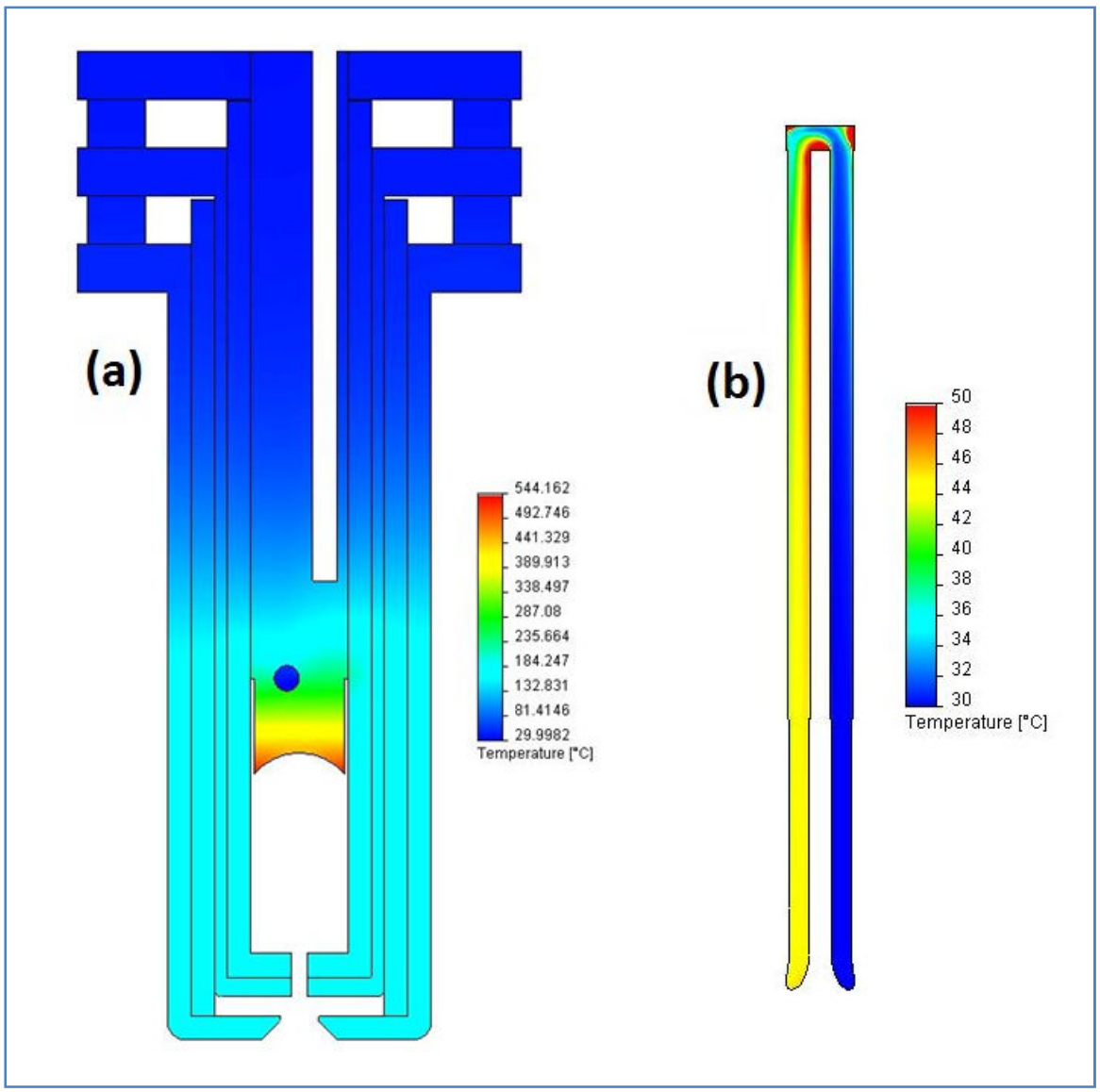

Figure 3.3 – (a) The initial cathode geometry in the plasma gun. The CFD simulation results for the gun and the cooling loop (b) are shown. The maximum temperature on the cathode is found to be 544 $^{\circ}$C. The heat load on the face was 1 kW, and the flow rate was 0.22 gal/min of water at 30°C

Any computer simulation must be verified, as a number of errors can arise during the simulation that give invalid results. With CFD a number of checks can be performed at the end of the simulation. A simple and accurate check for a CFD simulation involving heat transfer is to check if the flow rate is sufficient to remove the heat, by the thermodynamic relation

$$\mathbf{Q} = \dot{\mathbf{m}}\mathbf{c}\Delta\mathbf{T} \tag{6}$$

Where 'Q' is the heat load on the cathode, '$\dot{m}$' is the mass flow rate, 'c' is the specific heat of the water, and 'ΔT' is the change in temperature through the cooling loop. The heat removed 'Q' is 1000 W, and 'c' for H_2O is about 4179 J/kgK. '$\dot{m}$' was measured over a range of values, from roughly 0.22 gal/min to 0.30 gal/min. The lowest value was used in the simulation for more conservative results (0.22 gal/min is roughly 0.014 kg/s since 1 gal/min of H_2O is equal to 0.0639 kg/s). The temperature difference is then

$$\Delta\mathbf{T} = \frac{\mathbf{Q}}{\dot{\mathbf{m}}\mathbf{c}} = \frac{\mathbf{1000\ W}}{(\mathbf{0.014\ kg/s})(\mathbf{4179\ J/kg{\cdot}K})} = \mathbf{17.09}℃ \tag{7}$$

This compares decently with the 14.5 ± 4℃ found in the simulation (Figure 3.3). The slight difference is likely due to poor meshing and would lead to a higher temperature in the copper (the simulation fails to remove enough heat). Increasing the mesh would help with the accuracy and increase the computational time.

A new cathode was designed for a second simulation, which showed a maximum temperature of 450℃, well below the melting point of Copper and more acceptable than the previous simulation. This was done by bringing the cooling loop significantly closer to the heated face (as shown in Figure 3.4). A rounded edge was also added to the hemispherical face to reduce the sharp edges and help contain the heat. Additionally, by changing the temperature scale on the cooling loop in Figure 3.4 to a maximum of 100℃, it is possible to check for nucleation, or the boiling of water. The vapor pockets that develop can

lead to erosion when combined with turbulence, but fortunately the simulation does not show any nucleation.

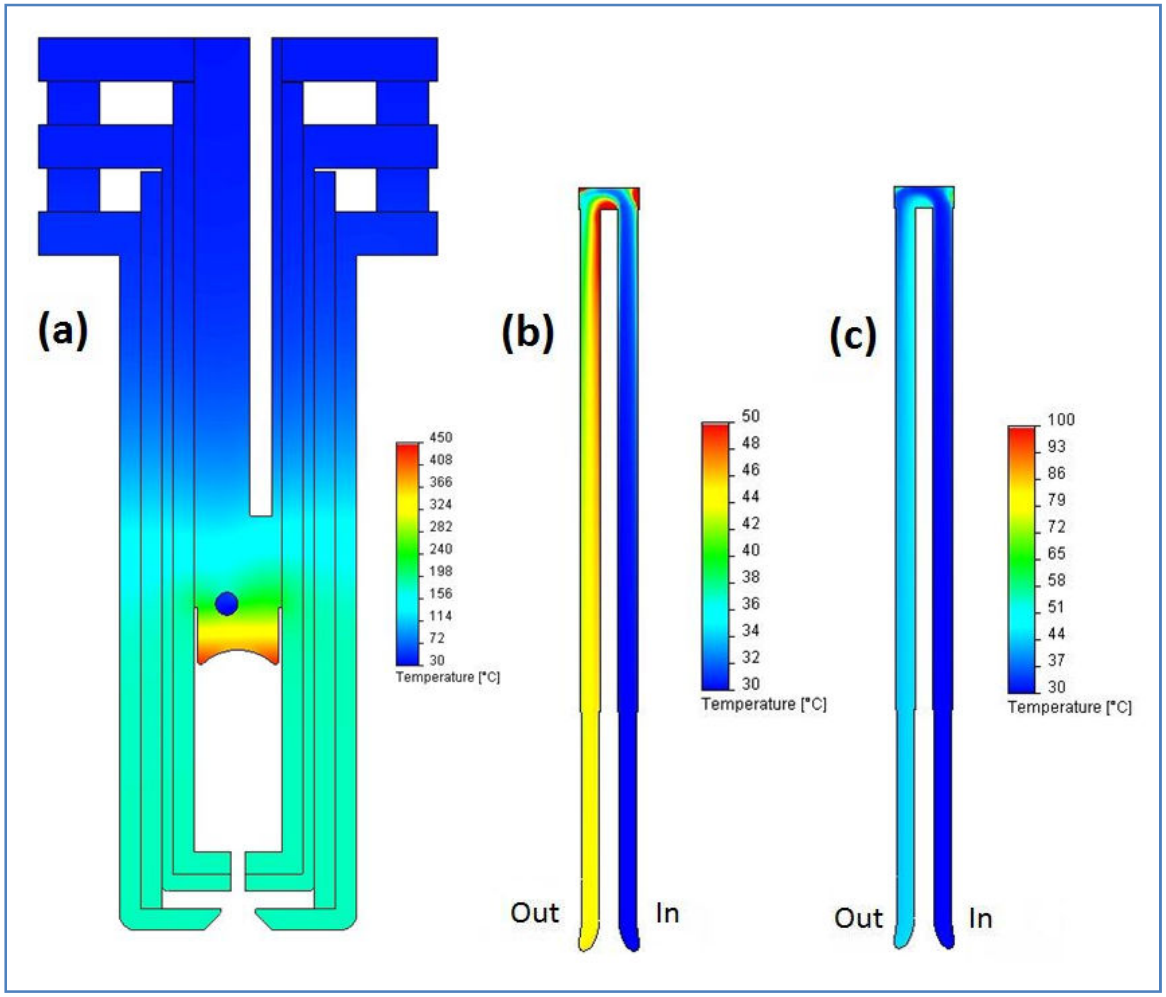

Figure 3.4 - The second simulation with a modified cathode shown in the plasma gun (a). The cooling loop (b) was brought closer to the heated cathode face, and rounds were added to the hemispherical face. The cooling loop shown in (c) is identical to (b) except for its temperature scale, which was increased to 30℃ to check for nucleation. All other simulation parameters are identical to the first simulation (0.22 gal/min flow rate at 30℃).

The temperature distributions appear to be acceptable, and the balance equation (Eq.7) gives the same ΔT as in the first simulation (the same mesh was used so the results could be accurately compared).

3.1 Simulation of the resulting thermal stresses

Now that the thermal and CFD simulation has acceptable results, the thermal stresses must be checked. The copper cathode temperature can increase by over 400°C, and the surrounding alumina and steel tubes can increase significantly as well. This increase leads to expansion in the materials, according to the thermal expansion coefficient of the material and the rise in temperature. Copper has a thermal expansion coefficient of about $16.5 \times 10^{-6} K^{-1}$, while steel has an expansion coefficient of about $17.3 \times 10^{-6} K^{-1}$. Alumina has a fairly low coefficient by comparison at $8.0 \times 10^{-6} K^{-1}$. [17]

With the copper expanding more rapidly, it could apply pressure against the alumina tube, which will expand less. This is accounted for in the model slightly by removing some material at the face of the cathode allowing for some expansion. Nonetheless, if expansion occurs in any of the materials, stresses will develop. Due to the thermal gradients, these stresses can be difficult to calculate, so computer modeling is again used. The FEA method is used by COSMOSWorks software to calculate the stresses throughout the plasma gun. [18]

The stresses to be calculated are the Von Mises stresses. In complex loading conditions, such as thermal gradients in three dimensions, the Von Mises stresses are calculated. Although the stresses at a given point may appear acceptable along the x, y, and z coordinates, the combination of the stresses may result in a stress with a larger magnitude. The Von Mises stress is found by the following equation [19]

$$\boldsymbol{\sigma_v} = \sqrt{\frac{(\boldsymbol{\sigma_1}-\boldsymbol{\sigma_2})^2+(\boldsymbol{\sigma_2}-\boldsymbol{\sigma_3})^2+(\boldsymbol{\sigma_1}-\boldsymbol{\sigma_3})^2}{2}} \quad (8)$$

where σ_1, σ_2, and σ_3 are the principal stresses. The principal stresses relate to the stresses along the coordinate axis by the following relation

$$\boldsymbol{\sigma_{1,2}} = \frac{\boldsymbol{\sigma_x}+\boldsymbol{\sigma_y}}{2} \pm \sqrt{\left(\frac{\boldsymbol{\sigma_x}-\boldsymbol{\sigma_y}}{2}\right)^2 + \boldsymbol{\tau_{xy}}^2} \quad (9)$$

where τ_{xy} is the shear stress in the x-y plane. [20]

To find the resulting Von Mises stresses the results of the second CFD (Figure 3.4) thermal simulation were imported into the COSMOSWorks software. These results are shown in Figure 3.5. The ceramic tube has excellent compressive strength (2600 MPa or approximately 375 ksi), but when subjected to expansion from the Copper cathode or its own expansion, the stresses are largely tensile. The tensile strength of alumina is significantly lower at 43,500 psi. For this reason, the stresses found by the initial FEA simulation were plotted and scaled to the tensile strength of alumina to check for failure. These initial results (Figure 3.5) were discouraging, as they show a significant portion of the alumina tube to be above point of tensile failure.

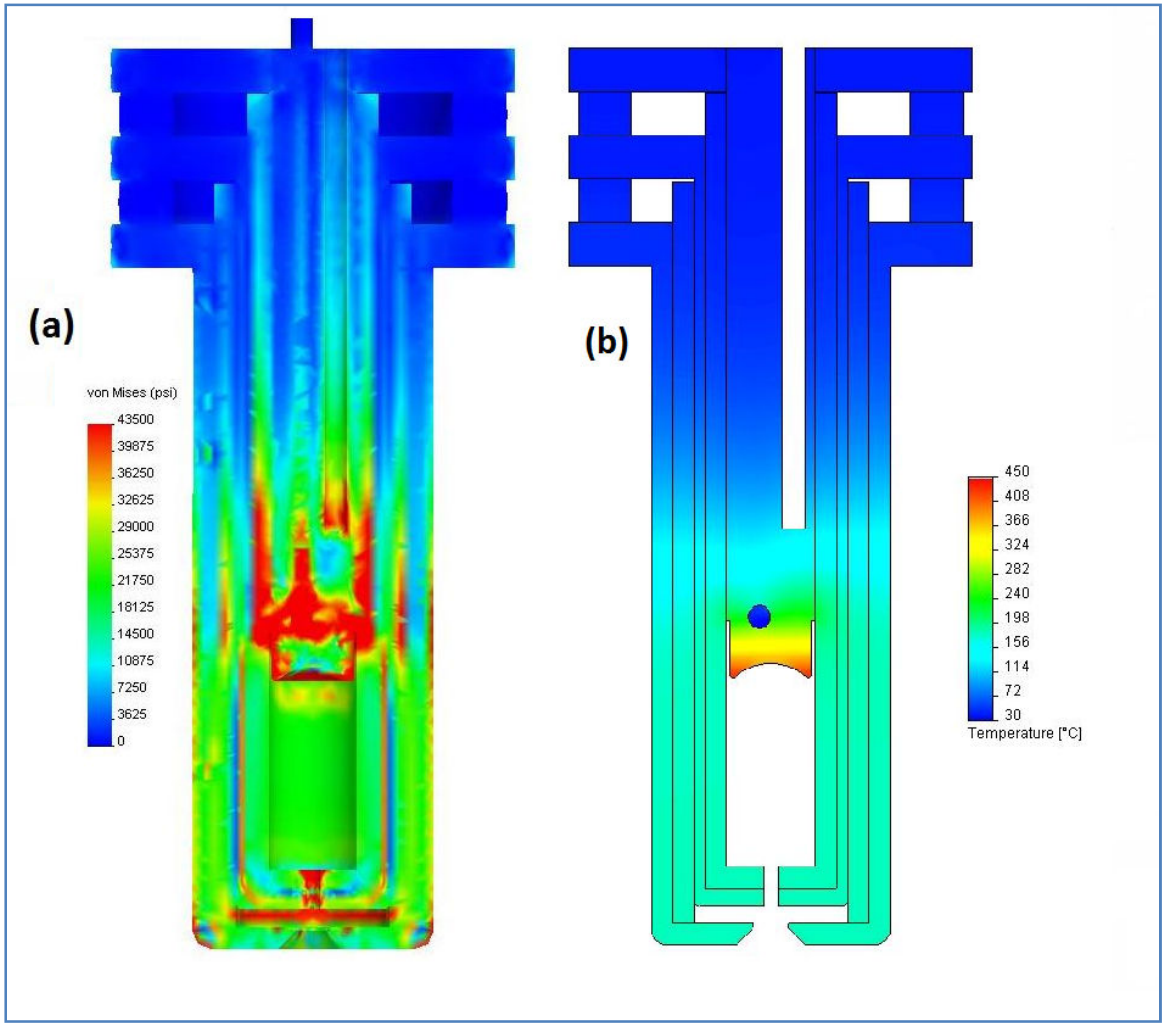

Figure 3.5 – The initial stress simulation using the second CFD simulation results (b). The Von Mises stress plot (a) was scaled to the tensile strength of alumina (~43,500 psi). This plot suggested the alumina tube would crack and fail from the heat load.

The first simulation in Figure 3.5 shows a concentration of stress after the cut around the cathode. Another simulation was setup that has a longer cut which extends well into the cooling loop. This allows less heat to escape the cooling loop, and also prevents expansion into the alumina tube. The results of this simulation, shown in Figure 3.6, show that nearly all the stress is eliminated by increasing the cathode cut. Further reduction would reduce the stress further, but would also raise the possibility of interfering with the hydrogen gas feed.

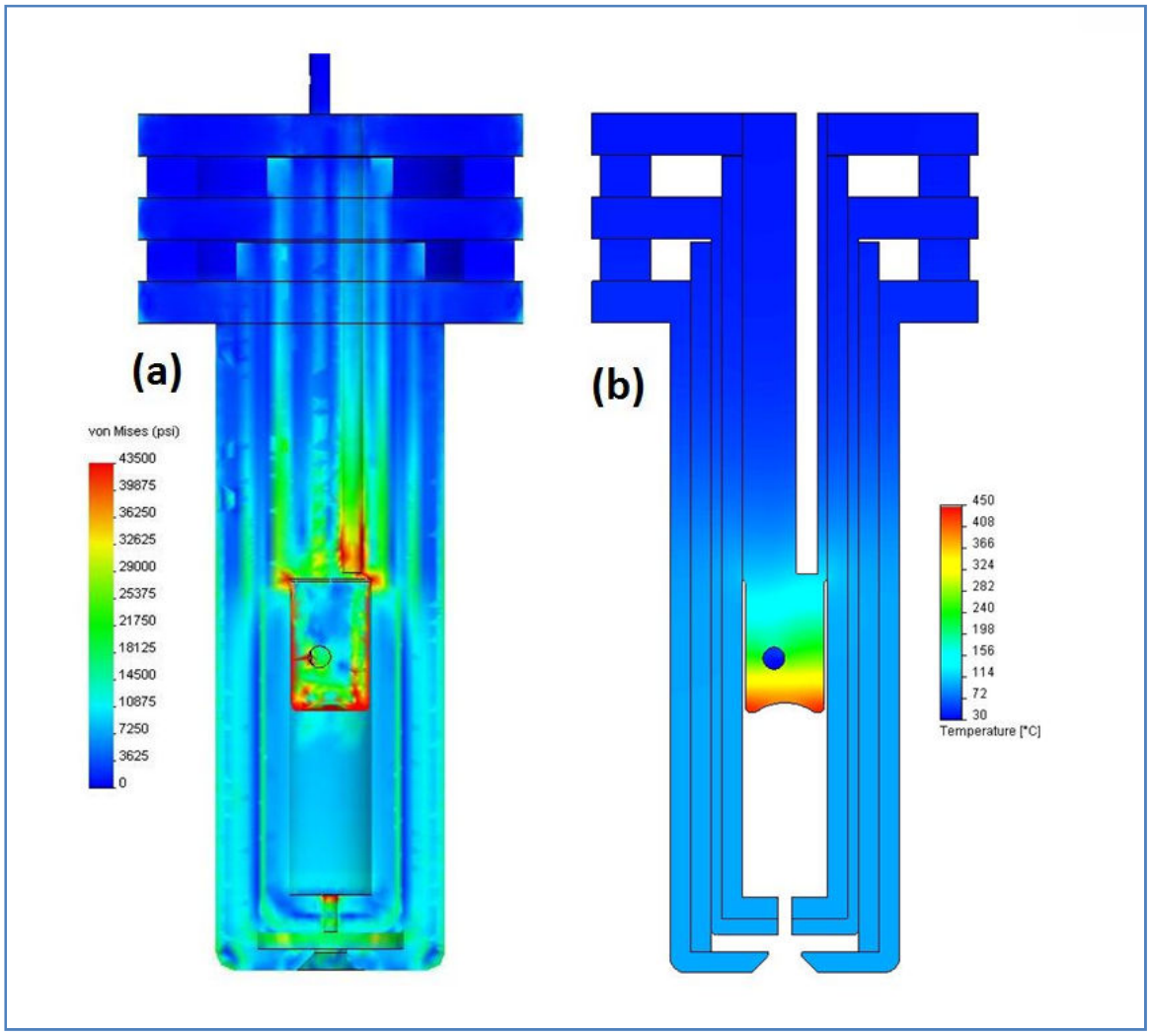

Figure 3.6 - Results of the second thermal stress simulation. The CFD simulation shown in (b) was run using the same parameters as the simulation shown in Figure 3.4, but with a modified cut on the cathode. This modified cut allowed for concentration of heat and much less thermal expansion into the alumina tube, virtually eliminating the stress found in the results of the first simulation.

While the simulation shown in Figure 3.6 demonstrates a working design thermally and mechanically, it would also be beneficial to increase the surface area of the cathode to increase the plasma current (from the increased ejected secondary electrons). A parabolic appearing cathode face was designed

which was shown through thermal and mechanical modeling to meet all design criteria. The cross section of this CFD Thermal simulation is shown below in Figure 3.7.

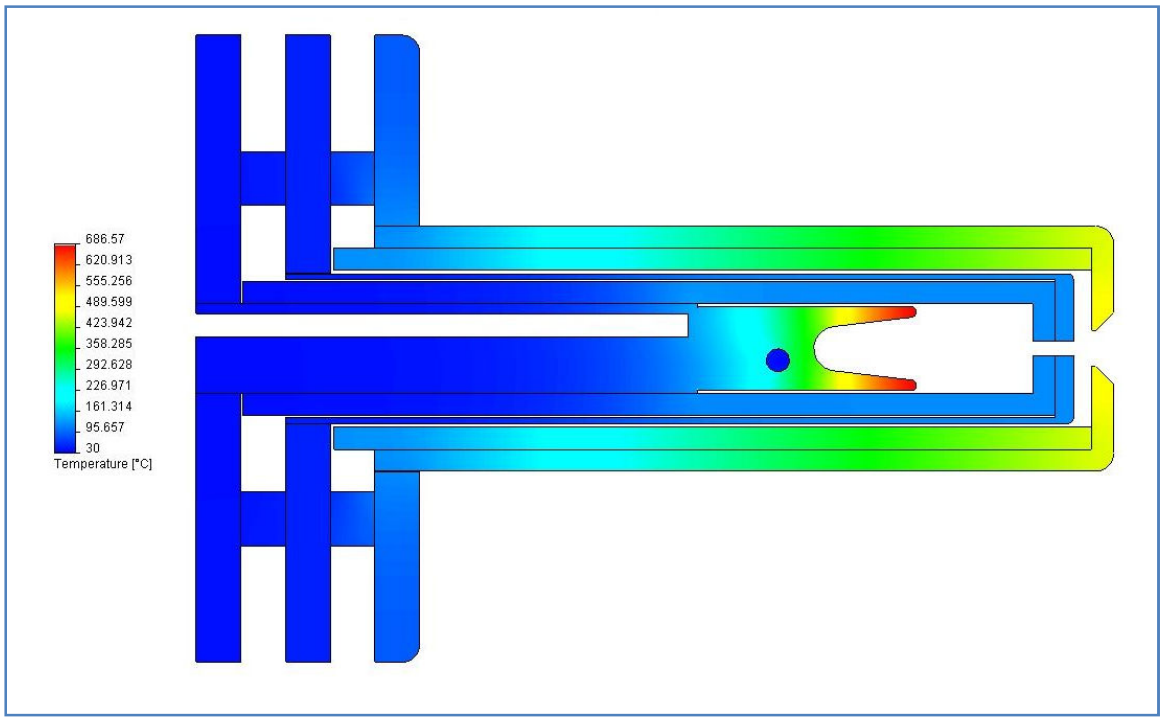

Figure 3.7 - The final design of the plasma cathode, showing a parabolic-like face for improved secondary electron emission. This design is marginally acceptable thermally, with a maximum temperature close to 700°C, but is instead optimized for ion and plasma current.

4. Integration of the Plasma Gun into the Ion Source

With the design of the plasma gun finalized by simulation, it is important to see how the gun integrates with the ion source itself. How the extracted particles interact with the plasma is a complicated process that is very difficult to predict. This interaction is something that is best found by experimental methods – that is, actually using the plasma gun with the ion source to make assessments. Before this is done, however, it is useful to characterize the behavior of the plasma gun. With an extraction electrode built into the design of the plasma gun, it is possible to vary the energy of the exiting plume of particles. This permits the control of the plume divergence. Additionally, an extractor electrode could allow for the selective extraction of particles, either electrons or ions. Simulation of this extraction process allows for guidance with future experimentation.

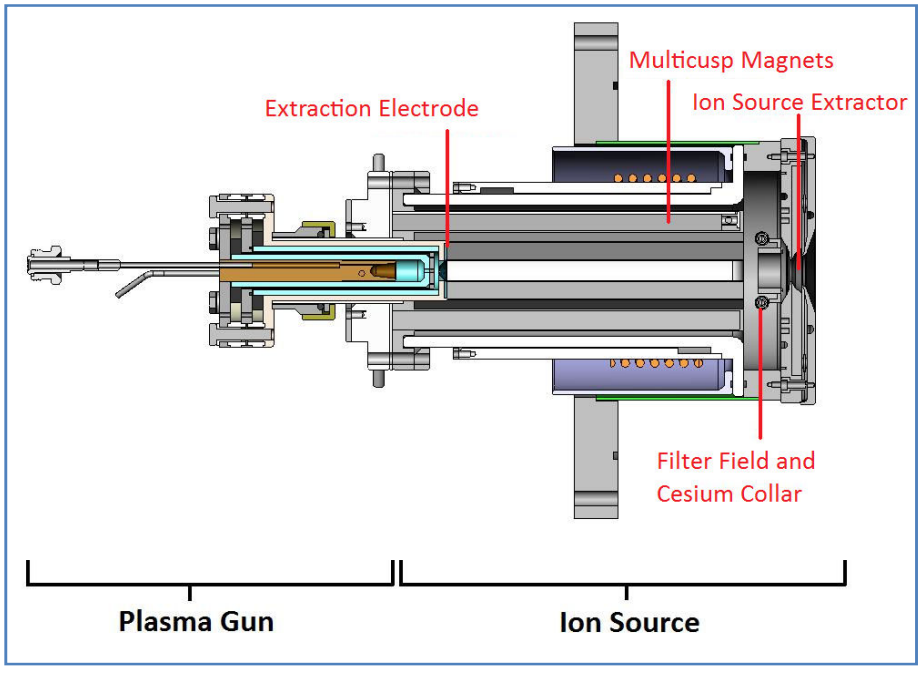

Figure 4.1 - Section view of the ion source assembly with the plasma gun attached. The plasma plume from the gun can be controlled by varying the potential of the extraction electrode. The divergence, energy, and the particle species of the plume can be controlled with this extraction electrode.

4.1 Ion Extraction

At the most basic level, extracting an ion or electron from a plasma is a relatively simple process. An electrode is positioned in front of an aperture which contains plasma. If a potential is applied to this electrode, species of the opposing charge will be extracted from the plasma. To design a minimally diverging beam that is as parallel as possible (minimal divergence) requires much more work, with careful consideration into the potentials of the electrodes as well as the geometry of the electrodes themselves.

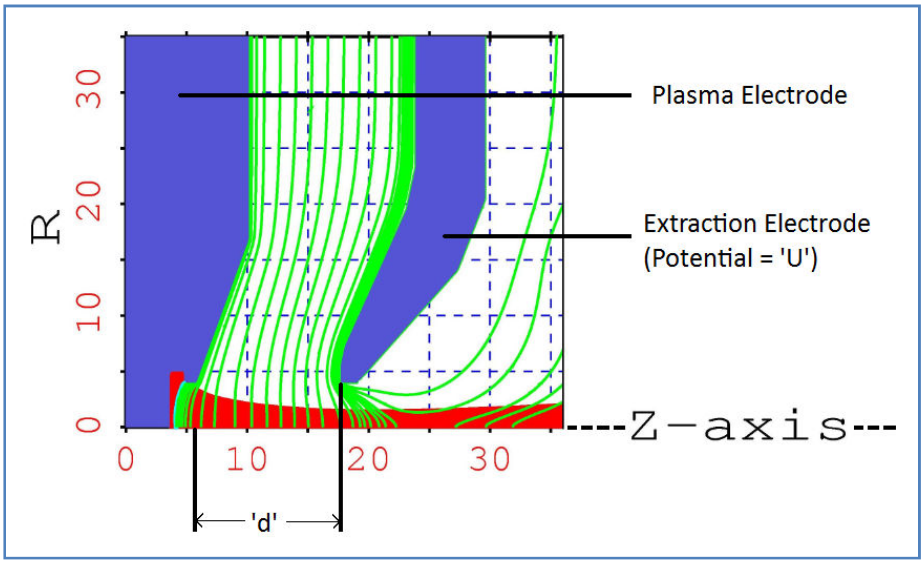

Figure 4.2 – A computer simulation of proton extraction from a plasma using the PBGUNS (Particle Beam Gun Simulation) code (see Ref. (21)). The red stream depicts the ion trajectories, and the green lines are the equipotential field lines.

Additionally, there are current limitations for a given potential of the extraction electrode, given by the Child-Langmuir law,

$$j = \frac{4}{9}\epsilon_0 \left(\frac{2q}{m_i}\right)^{1/2} \frac{U^{3/2}}{d^2} \tag{10}$$

where ‘j’ is the maximum attainable current density, ‘q’ is the charge of the ion, ‘m_i’ is the mass of the ion, ‘U’ is the extraction electrode potential, and ‘d’ is the gap between the plasma electrode and the extraction electrode (as shown in Figure 4.2). For the plasma gun this law states that even if there is current in the plasma available to extract, there is a peak current which can be extracted which depends on the extraction potential. For an increased extraction potential, we can expect a corresponding increase in beam current to a peak value given by (Eq. 11). [22]

Also an important characteristic of an ion beam is the perveance of the beam, P,

$$\boldsymbol{P = IU^{-3/2}\left(\frac{A}{\xi}\right)^{1/2}} \qquad \textbf{(11)}$$

Where ‘I’ is the ion current, ‘U’ is the same extraction potential, ‘A’ is the atomic mass of the extracted ion, and ‘ξ’ is the ion charge state. This perveance is calculated from the conditions set in (Eq. 11). [22]

4.2 Emittance

For the plasma gun we are not so concerned about the beam quality parameters such as perveance, and brightness, since our goal is more or less to flood a given volume with particles. For the plasma gun, the parameter we are interested in is the beam divergence, which is characterized by a quantity known as emittance.

Emittance is a yet another beam quality parameter, where at some designated point along the axis of the beam the diverging half angle of the beam ‘α’ is measured incrementally away from the axis. What results is a plot which consists of distance on one axis (often in mm) and divergence angle (mrad) on the other. A large emittance can correspond to either a largely diverging or converging beam. Often, since the resulting plot is elliptical, a factor of π is multiplied by the angle measure for convenience.

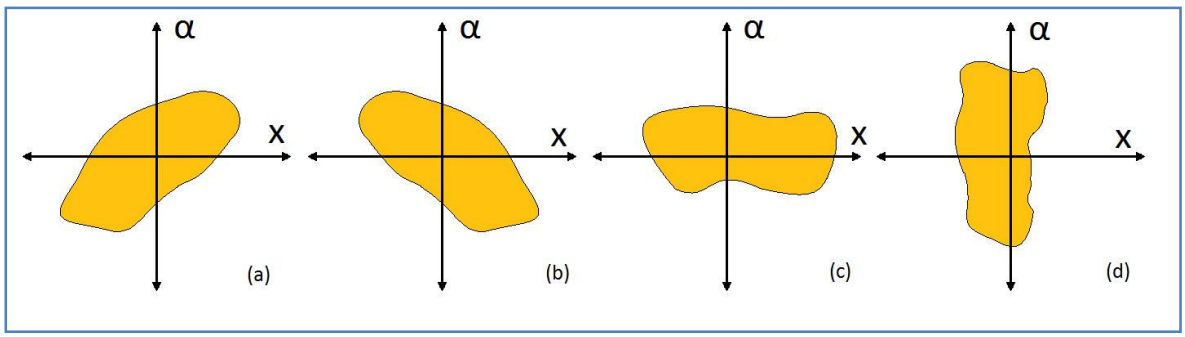

Figure 4.3 – Four emittance plots of a beam, showing the four possible cases of divergence. Plot (a) shows a divergent flooding beam, plot (b) shows a convergent beam, plot (c) shows a parallel beam which is ideal for many applications, and plot (d) shows a focus along the beam. This Figure is the work of the author but based closely on a Figure by R. Keller, in Ref. (22).

Aberrations in the beam can result from magnetic fields, collisions with electrodes, and other effects which are difficult to take into account in a simulation. Also, a beam has a thermal spread of energies which effects the distribution in the emittance plot. An example of a realistic emittance plot is shown in Figure 4.4.

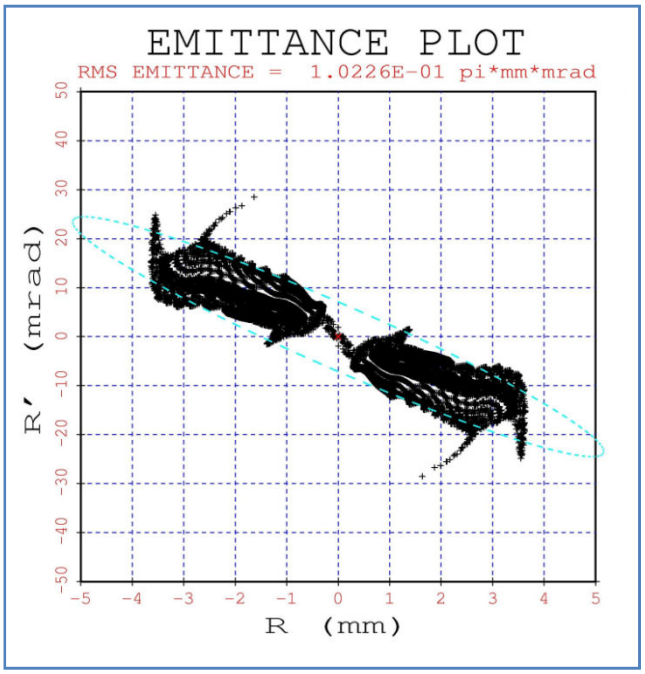

Figure 4.4 - An emittance plot generated from a PBGUNS simulation (see Ref. (21)) which takes into account a thermal spread of the ions. The ellipse outline shows the shape of a converging beam. This plot is generated from a point along the axis of the beam, 40 mm from where the plasma exits the ion source. The 'R' is the distance away from the axis at this point ('X' in Figure 4.3), and the R' is the angle measure at this point (alpha in Figure 4.3).

While the emittance plots provide a wealth of data, often what is desired is one statistical number of emittance given as a scalar value, for ease of comparison between different systems. This emittance is called the rms emittance, and is defined as

$$\epsilon_{\mathbf{rms}} = \left(\overline{\mathbf{x}^2}\,\overline{\mathbf{x}'^2} - (\overline{\mathbf{x}\mathbf{x}'})^2\right)^{1/2} \quad (12)$$

where '$\mathbf{x}'$' is the angle measured from a point '$\mathbf{x}$' away from the axis of the beam (at a designated point on the beam). The units for rms are given in (pi*mm*mrad) as shown at the top of Figure 4.4. From this simple scalar number, the shape of the beam can be determined anywhere forward from the point where the rms measurement was made.

4.3 Simulation of the Plasma Gun

Similarly to the fluid flow, heat, and thermal stress simulations, the characterization of the plasma beam can only be done numerically; even relatively simple processes can be computationally intensive. The PBGUNS code (Ref (21)) provides very exact simulations of plasma extraction, but requires knowledge of many plasma parameters in the ion source. This code will calculate the plasma meniscus (boundary between the plasma and extraction region) and the effects of the beam's charge (space charge) through a timely iterative process. However, for the plasma gun we do not need such extensive calculations since the two parameters we are most concerned about are divergence and emitted current. For such a simulation, every particle can be treated as independent from another particle, showing a basic "flight pattern". One computer program we use for these simplified calculations is the Simion code. [23]

Like many of the other codes used, Simion employs the Finite Element Analysis (FEA) method. A geometry is imported into Simion, or built from scratch, which is then meshed for running the FEA

simulation. Simion calculates the potentials in the simulation from the electrodes and an emitting surface is defined, similarly to PBGUNS. Figure 4.5 shows the completed mesh of the plasma gun in Simion.

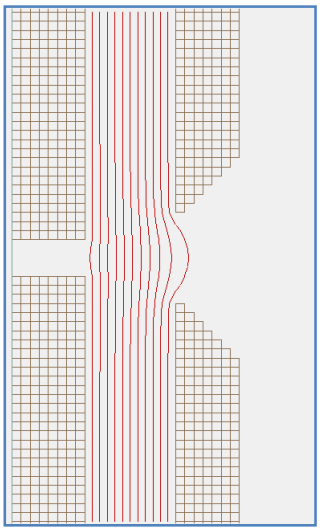

Figure 4.5 - A reduced and simplified model of the plasma gun in Simion, showing the completed mesh and equipotential line. The extraction electrode (right) is at 300 V.

To characterize the emittance of a beam in Simion, it was necessary to create a user program (Simion PRG code), since the capability was not built into the original Simion program. Each particle's coordinates and velocity components were tracked and logged. After the particles exited the simulation domain at the right of the mesh, their components were logged in a database, and the averages taken to find the rms emittance as in (Eq. 13). Here is the beginning of the user programming code, where the particle parameters are recalled and manipulated, and finally stored in an array. For the complete code, refer to Appendix C.

```
LBL emittance                ; start of data manipulation

        RCL Ion_Py_mm        ; load the particles y position (in mm units)
        RCL ion_number       ; load the particle's designated number
        asto y               ; store in array 'y' (i.e. [ 1 , 1.234 mm ] )

        RCL Ion_Vx_mm        ; find particle's x-velocity and store with number
        RCL ion_number       ; in array 'velocityx'
        asto velocityx
```

```
RCL Ion_Vy_mm          ; same, but for velocity in 'y'
RCL ion_number
asto velocityy

RCL Ion_Vy_mm          ; load particle y-velocity in mm/s
RCL Ion_Vx_mm          ; load particle x-velocity in mm/s
Divide                 ; do Vy / Vx
Sto Yprime                    ; store result as yprime

RCL Yprime             ; load the yprime again
RCL ion_number         ; load the associated ion number
asto yprime            ; store result in yprime array
```

The lead developer for the Simion company, David Manura, expressed interest in incorporating an emittance code into the final release of Simion. He transferred the code to the Lua programming language, thereby improving the speed and reducing the size of the code. This code is also shown in Appendix C. [24]

The plasma gun simulation in Simion showed the capability for varied energy extraction with very good control over the divergence of the beam. With a low voltage power supply up to 500 volts, it would be possible to either flood the entire ion source plasma chamber, or create a higher energy beam which interacts more with the cesium collar area. The results of the simulation are shown in Figure 4.6.

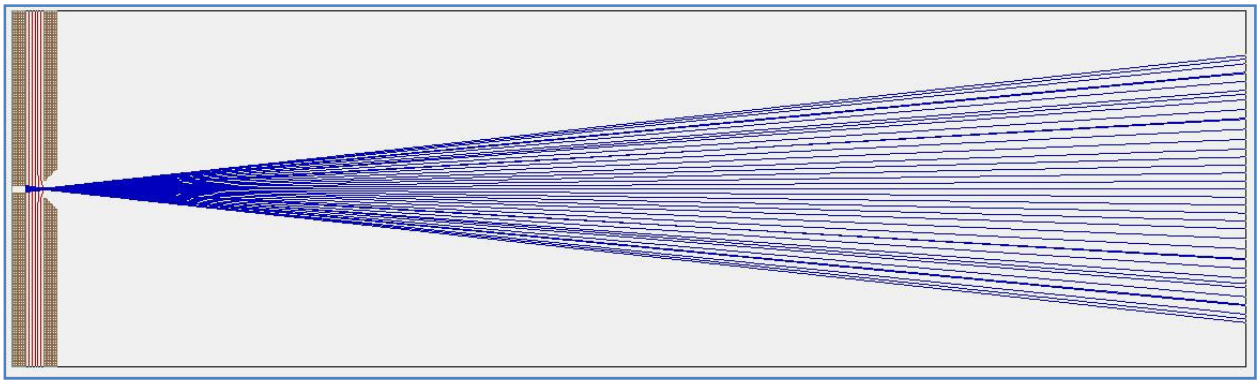

Figure 4.6 - Extraction of thermal electrons (0.1 eV) from the plasma gun at an extraction voltage of 100 V. The simulation shows the beam has a wide divergence, which should allow for greater interaction with the ion source plasma. The added electrons and ions should interact with the ion source plasma boosting performance, although this remains to be experimentally verified.

5. The Completed Plasma Gun

5.1 Mechanical Performance

The goal of designing a new plasma gun was to create a modular assembly that could be attached and detached to the back of the SNS ion source with ease. The plasma gun also needed extraction capability and the copper cathode capable of sustaining 1 kW of power. The CFD, thermal, thermal stress, and particle trajectory simulations discussed in this report all demonstrated a working model of the plasma gun. With the plasma gun design verified by computer codes, the various parts were sent out for fabrication and assembly. The completed model is shown in Figure 5.1.

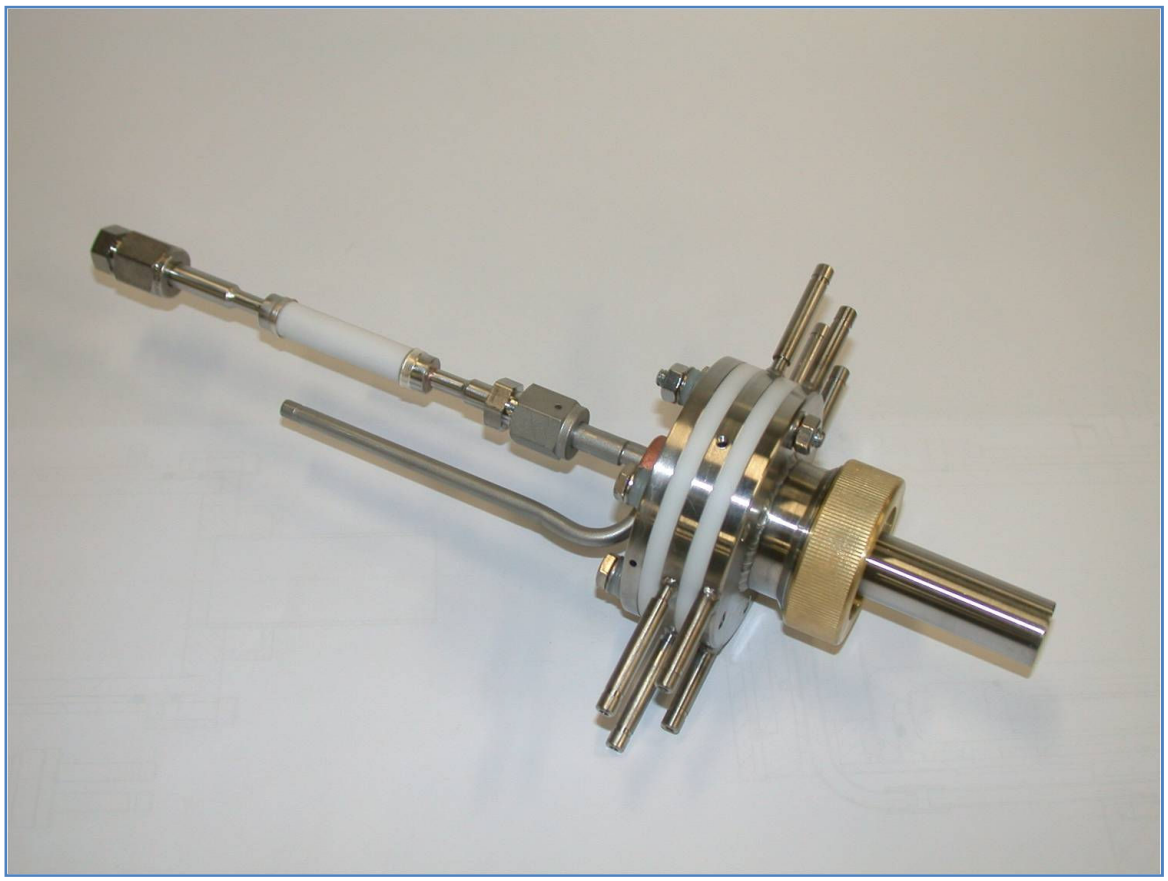

Figure 5.1 - The completed plasma gun, showing the insulated VCR gas feed, and multiple water coolant connection lines.

The mechanical design performed as expected, although two problems were discovered. The viton gaskets did not have an adequate surface finish and could not create a proper vacuum seal. Syd Murray (a member of the SNS ion source team) corrected this by removing the gaskets and polishing the surface by hand. The other issue was with the 1/8 inch cathode cooling lines, which were too fragile and easily broke if adjusted. The cathode end was redesigned by ORNL engineer Danny Crisp to accommodate two ¼ inch water lines, which were much more robust (see appendix A for the cathode drawing). Besides these two issues, the gun performed as expected with respect to the mechanical design. The gun has survived for months of operation without failure, confirming the validity of the computer simulations. Figure 5.2 shows the plasma gun attached to the back of the ion source.

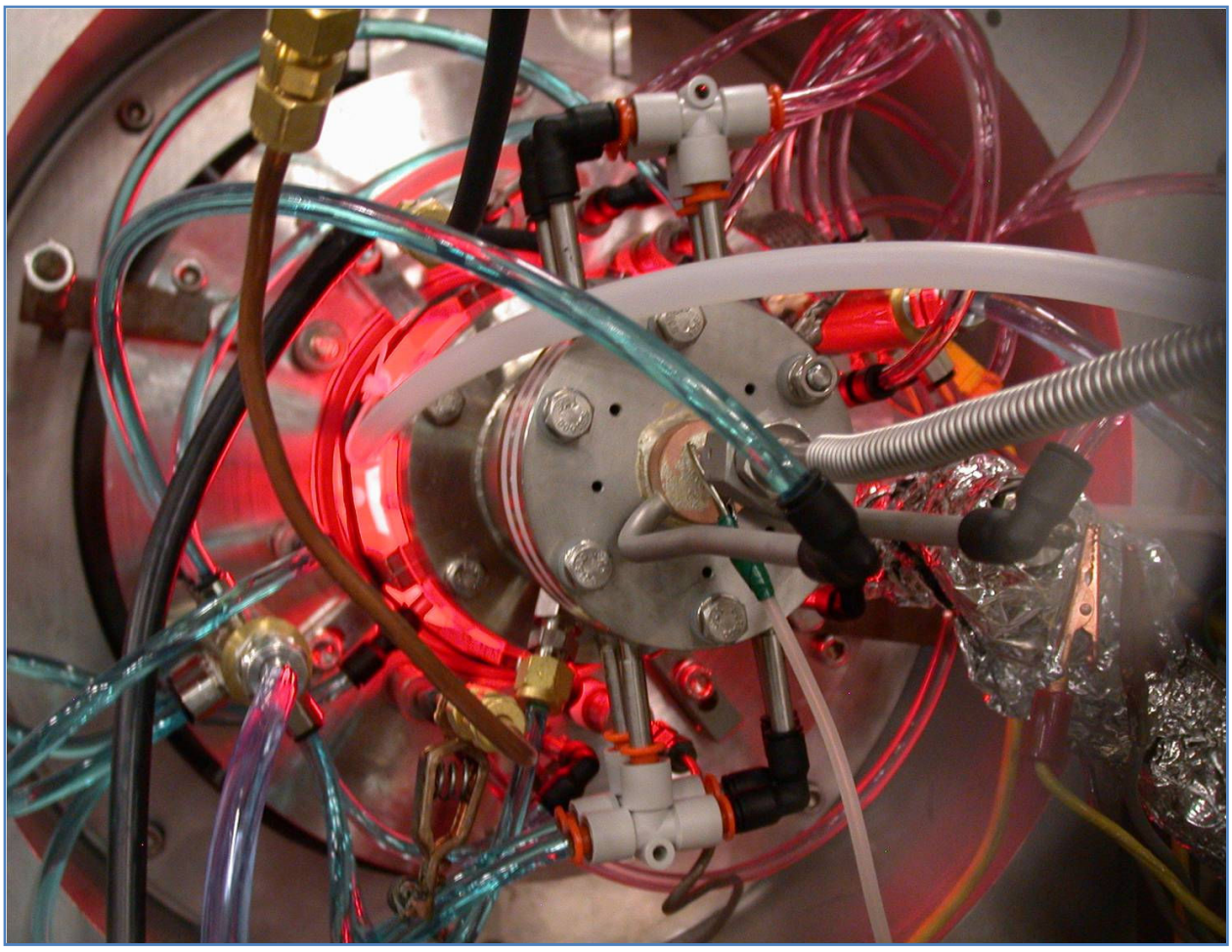

Figure 5.2 – The plasma gun attached to the back of the ion source, which glows red from the ignited plasma.

5.2 Operation of the Plasma Gun

With the plasma gun completely assembled and repaired, testing could begin. Jerry Carr Jr., a graduate student at ORNL, created a plasma gun test stand to characterize the behavior of the plasma gun before attaching it to the ion source. This test stand consisted of a large turbomolecular vacuum pump, a faraday cup for beam current analysis, a camera, and a floating power supply for the gun. This was enclosed in a grounded faraday cage, as shown in Figure 5.3.

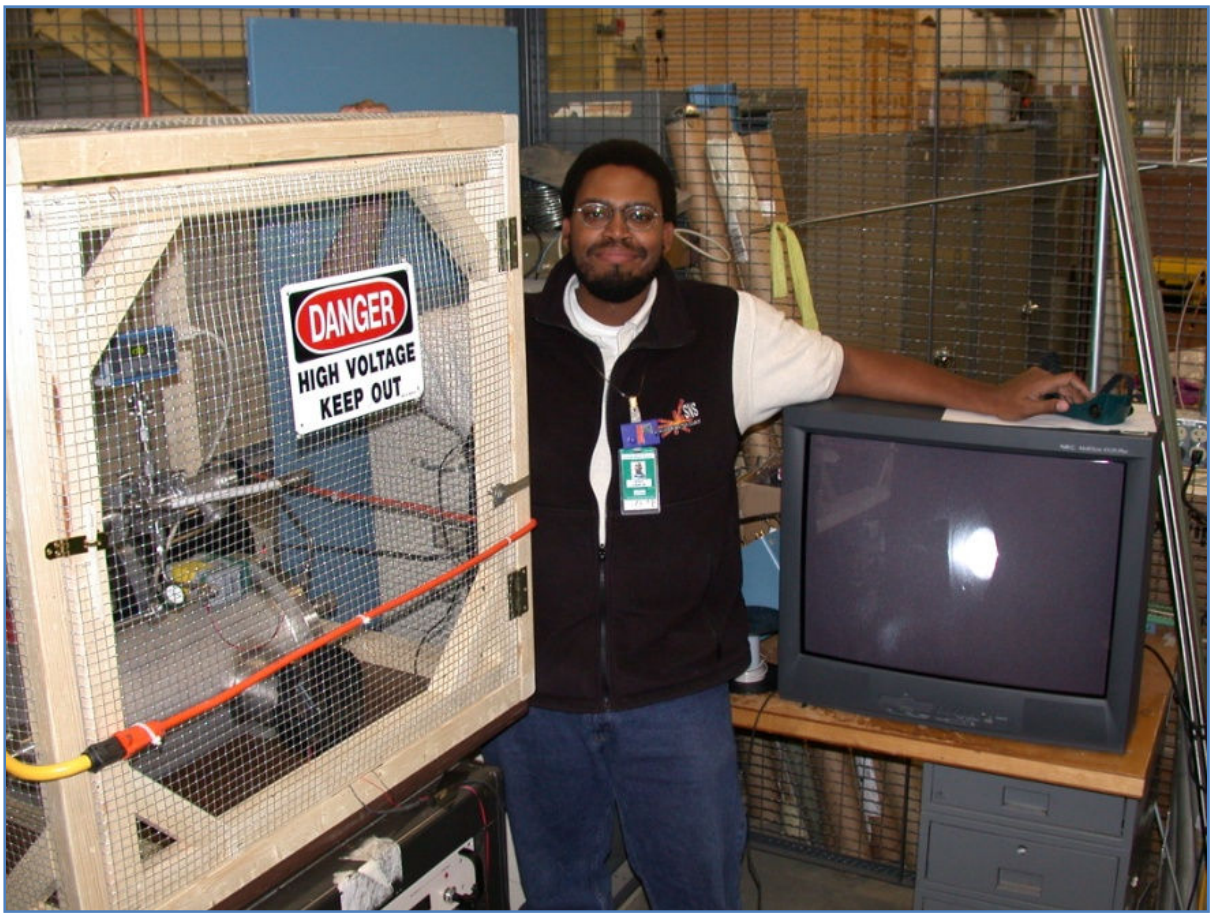

Figure 5.3 - Plasma source test stand and graduate student Jerry Carr Jr. The vacuum chamber which tests the plasma gun can be seen inside the faraday cage. The ion gauge and camera can also be seen, along with the video seen on the television of the operational plasma gun.

The plasma gun was tested at various pressures, extraction voltages, and currents. A common graph to characterize the performance of the plasma gun is a "VI" graph, which shows extraction voltage with the current collected by the faraday cup. This data was collected for several pressures, as shown in Figure 5.4.

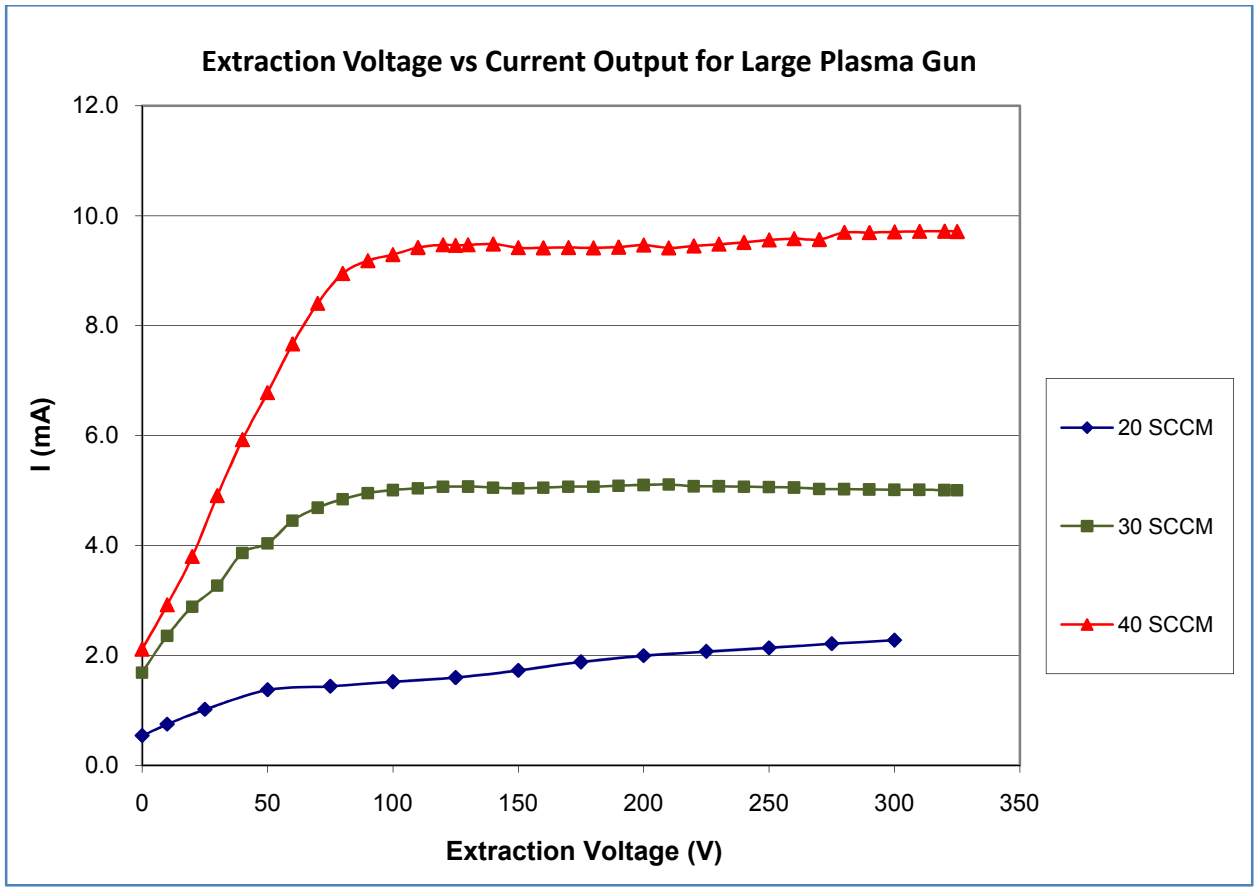

Figure 5.4 - Extraction voltage vs. collected current for the large plasma gun. The cathode voltage is held at a constant 1 kV. The graph shows data collected at three different gas flow rates of H2 gas (measured in standard cubic centimeters per minute (SCCM)). This data was collected by Jerry Carr Jr.

It can be observed from Figure 5.4 that there is a strong dependency on the gas flow rate. It appears that for a given gas flow, there is a maximum current capable of being extracted. The Child-Langmuir law given by (Eq. 11) cannot describe this as it only applies to a saturation of current given by a constant extraction potential (while ignoring the effects of pressure or gas feed). Intuitively, it would appear that

the maximum current is not at all dictated by the extraction potential but rather the amount of ions available, which would be dependent primarily on the gas feed. Therefore, this graph suggests that the plasma gun current is not limited by the extraction potential, but rather the amount of gas that can be fed while still maintaining a stable plasma. A graph of the maximum extracted current versus the gas feed rate (Figure 5.5), shows this dependence.

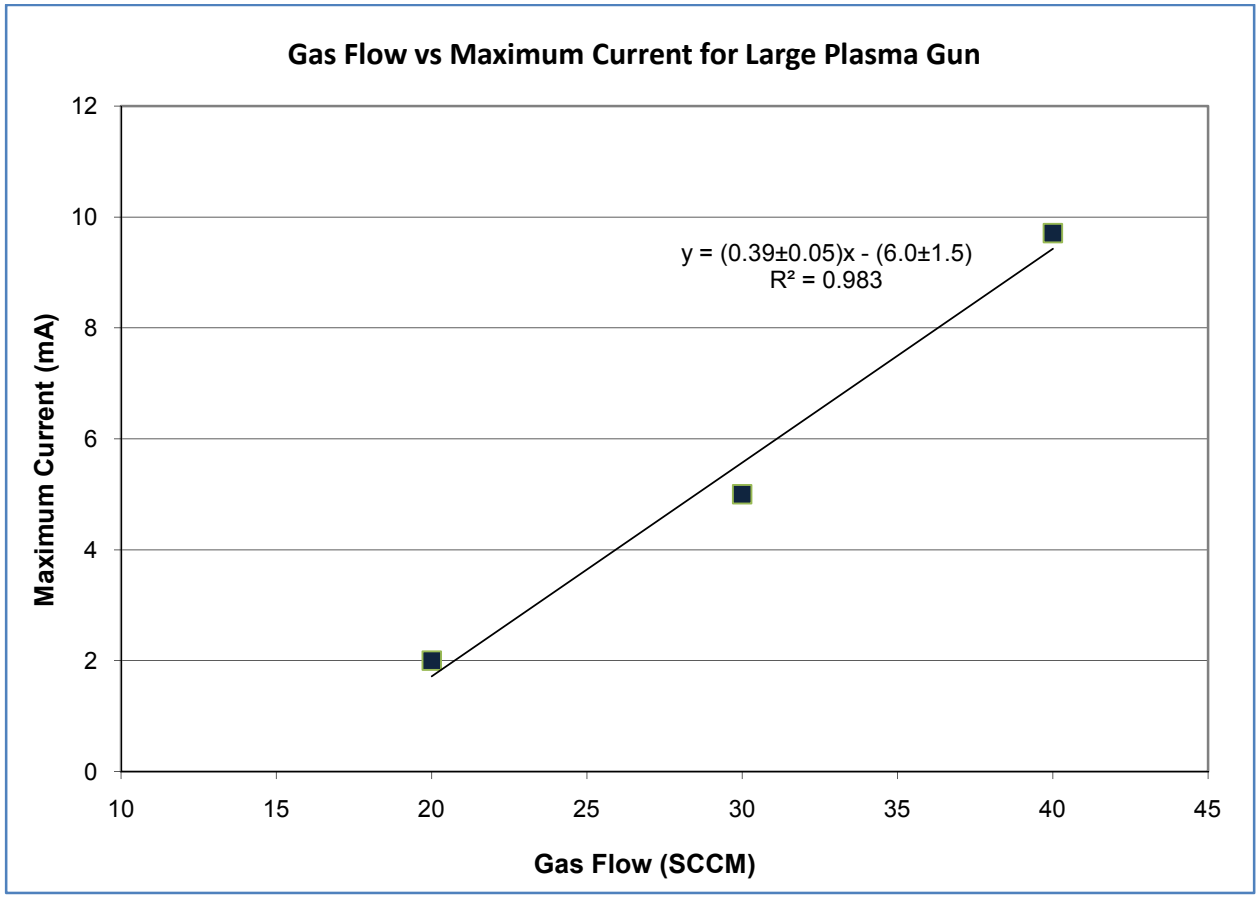

Figure 5.5 - The maximum attainable current in the plasma gun for a given gas flow. This data, taken from the data shown in Figure 5.4, shows a strong linear dependence. The equation superimposed on the graph is the best fit line for the given points.

As Figure 5.5 shows, there is a strong linear dependence between the gas flow rate and the maximum attainable current in the plasma gun. As mentioned, this is likely because the extraction potential range is so high that the Child-Langmuir law does not have an effect. If a plasma could remain stable for a large

gas flow rate and a supply of ions were available were extraction, we could expect the Child-Langmuir law to come into play and this linear dependence would saturate at some value given by (Eq. 11). In the case of a glow discharge plasma gun, this is not so straight forward to calculate since the plasma aperture is not at ground with respect to the extraction electrode. The Child-Langmuir law is suited for a grounded plasma electrode which emits no current when the extraction electrodes are not active. For this plasma gun, current is emitted even if the extraction electrode is held at ground potential with respect to the anode. Although the beam current limit cannot be calculated directly, some variant of the Child Langmuir law would be expected to apply which would create an upper limit for emitted beam current.

From Figure 5.4 we can see that the maximum current attainable for a given gas feed occurs at the highest extraction potential, which is what one would expect. Therefore, to find the maximum current the gun can deliver we took additional data by using the highest extraction potential while varying the gas flow rate, as shown in Figure 5.6.

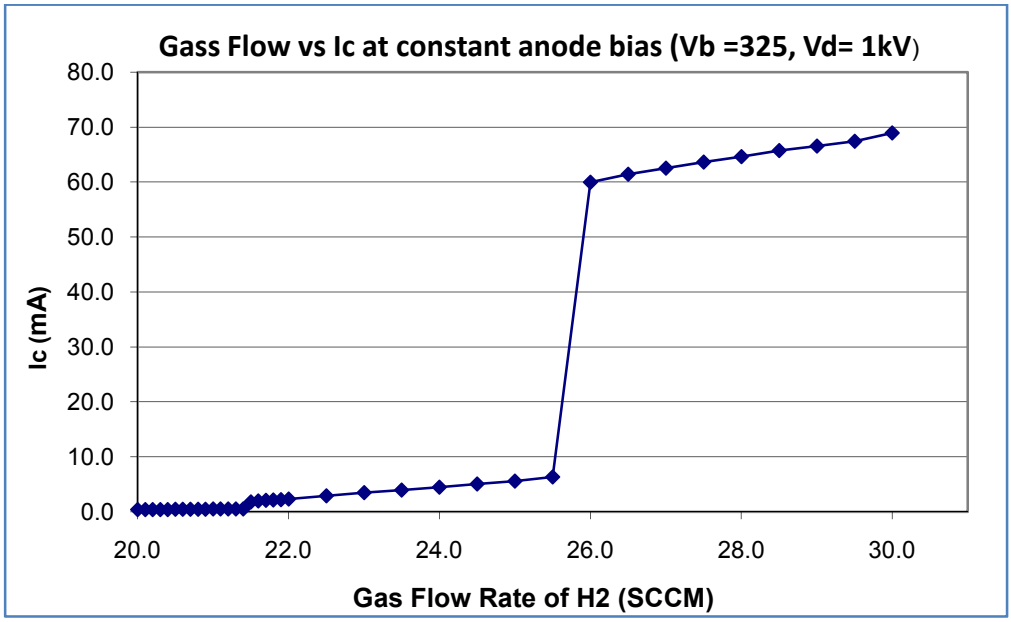

Figure 5.6 – This data was taken for a constant cathode and extraction voltage (Extraction Voltage = 325 V, Cathode Voltage = 1000 V). The gas flow was varied, and two distinct modes of operation can be seen. This data was collected by Jerry Carr Jr.

This data, taken by Jerry Carr, shows two abrupt transitions. The first transition occurred at approximately 21.5 SCCM of gas flow, and gave the appearance of a focused beam. The second transition was observed to occur at approximately 26 SCCM of gas flow, and the behavior was quite different, leading to a highly luminous discharge which "filled the entire vacuum chamber". The behavior of the plasma gun is somewhat mysterious, as the mechanism behind this "mode transition" is not at all understood. The data given in Figure 5.6 does not correspond with the data in Figure 5.4 and Figure 5.5, and shows presumably exaggerated beam currents. There are two possibilities here: the first is that there is a poorly understood mode transition within the plasma gun which leads to highly efficient operation and large beam currents; the second possibility is that there is a discharge occurring between the plasma gun and the faraday cup which would lead to erroneous data (see Figure 5.7). More data has to be taken to understand what is occurring within the plasma gun, and whether or not previous measurements were accurate.

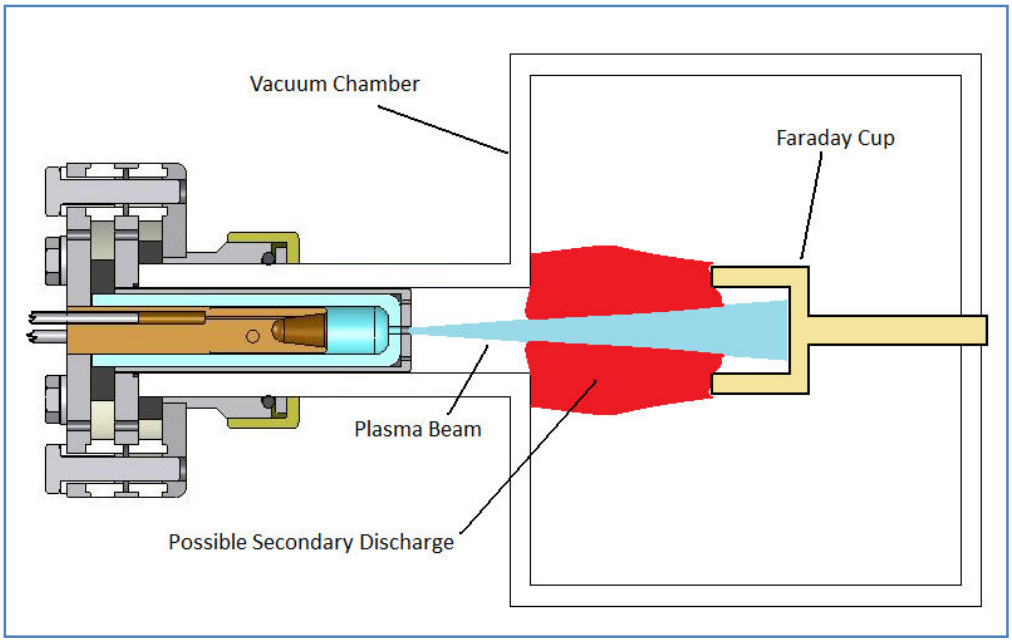

Figure 5.7 – This figure illustrates how a second discharge may have formed between the faraday cup and the vacuum chamber leading to erroneous data. The secondary discharge could account for the large increase in collected current if it were sustained simultaneously with the plasma beam discharge.

5.3 Conclusions

The mechanical design of the plasma gun met all the initial design criteria as discussed in section 2.1. The gun was found to be capable of handling 1 kW of power on the cathode face in simulation and survived all the initial tests without failure. Additionally, the modularity of the plasma gun allows for modifications to be made to the design with ease.

The foremost goal of this project was to create a plasma gun capable of providing more power than the prototype hemispherical plasma gun, while maintaining the ability to extract at varying energies. The data shown in this section, although somewhat contradictory, shows a maximum of either 10 mA (see Figure 5.4) or 69 mA (as shown in Figure 5.6). All the data, however, suggests large gains over the prototype's maximum current of 2 mA. It is expected that this increased plasma current combined with the extraction system will benefit the performance of the SNS ion source by increasing the H- ion current and improving the efficiency of the source. Indeed, it was found that in some cases the ion source current can increase by 50% (although this has yet to be seen at the SNS). How the plasma gun affects the performance of the ion source remains something to be experimentally tested.

Improvements to the performance of the plasma gun itself may be sought. The mechanical lifetime may be extended with careful materials selection to reduce ion sputtering of the cathode. Also, the effect of axial magnetic fields on the plasma gun has not been determined for this design. If a magnetic field was created along the axis of the plasma gun, the output may be greatly enhanced, as the literature suggests (see section 1.4). A careful study of the effects of extraction potential, gas feed, and magnetic field on the plasma gun current should be undertaken.

Appendix A: Relevant Engineering Drawings

As referenced in Chapters 2 and 5, several engineering drawings are included here to clarify design intent. The assembly drawings and minor components are not included. Please note that the scales given on these drawings are no longer accurate as the drawings are reduced in size to fit on the page.

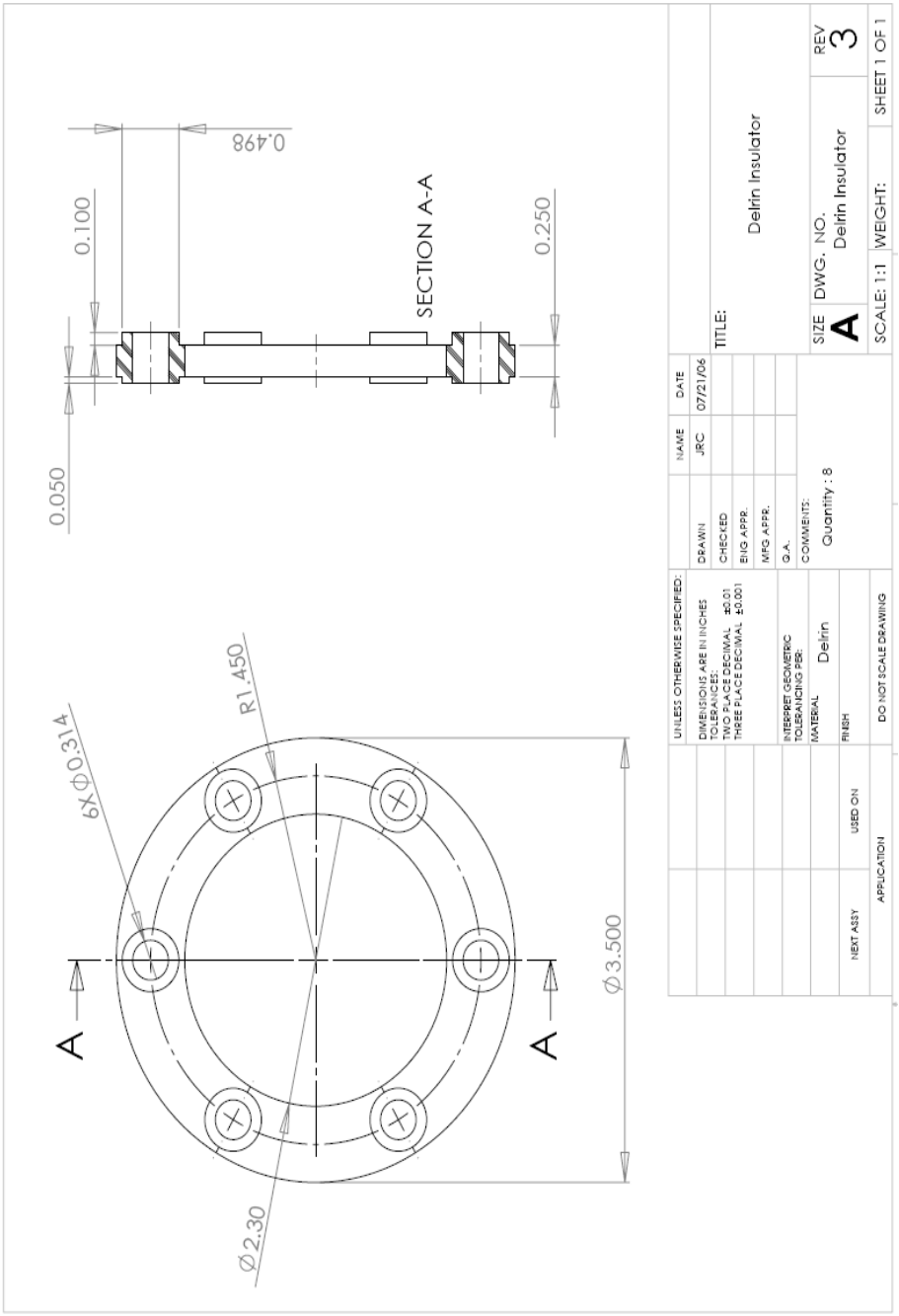

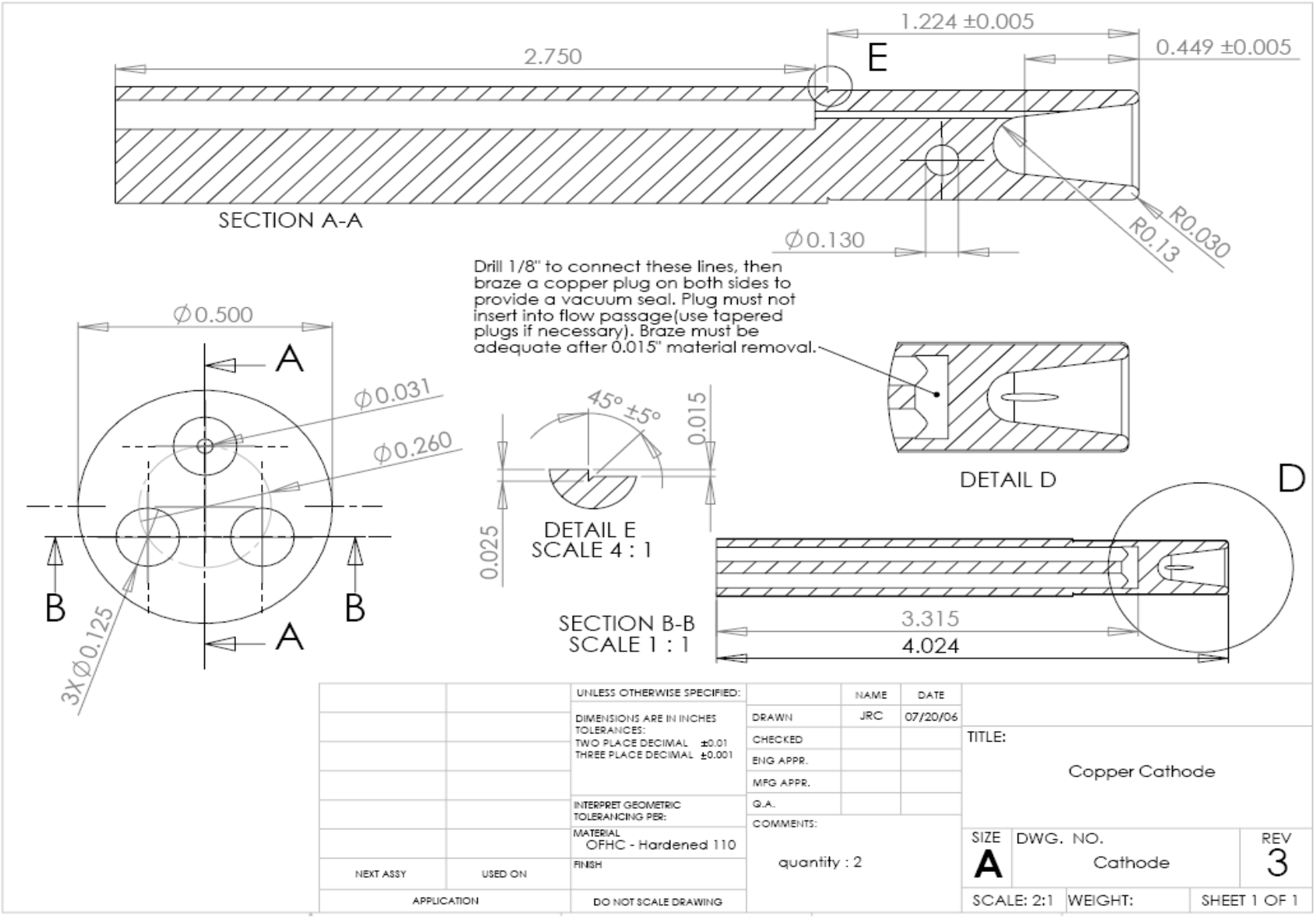
1.224 ±0.005
0.449 ±0.005
2.750
E
SECTION A-A
∅0.130
R0.030
R0.13
Drill 1/8" to connect these lines, then braze a copper plug on both sides to provide a vacuum seal. Plug must not insert into flow passage(use tapered plugs if necessary). Braze must be adequate after 0.015" material removal.
∅0.500
A
∅0.031
∅0.260
B
B
A
3X∅0.125
45° ±5°
0.015
0.025
DETAIL E
SCALE 4 : 1
DETAIL D
D
SECTION B-B
SCALE 1 : 1
3.315
4.024
UNLESS OTHERWISE SPECIFIED:
DIMENSIONS ARE IN INCHES
TOLERANCES:
TWO PLACE DECIMAL ±0.01
THREE PLACE DECIMAL ±0.001
INTERPRET GEOMETRIC TOLERANCING PER:
MATERIAL
OFHC - Hardened 110
FINISH
NEXT ASSY
USED ON
APPLICATION
DO NOT SCALE DRAWING
NAME
DATE
DRAWN
JRC
07/20/06
CHECKED
ENG APPR.
MFG APPR.
Q.A.
COMMENTS:
quantity : 2
TITLE:
Copper Cathode
SIZE
A
DWG. NO.
Cathode
REV
3
SCALE: 2:1
WEIGHT:
SHEET 1 OF 1

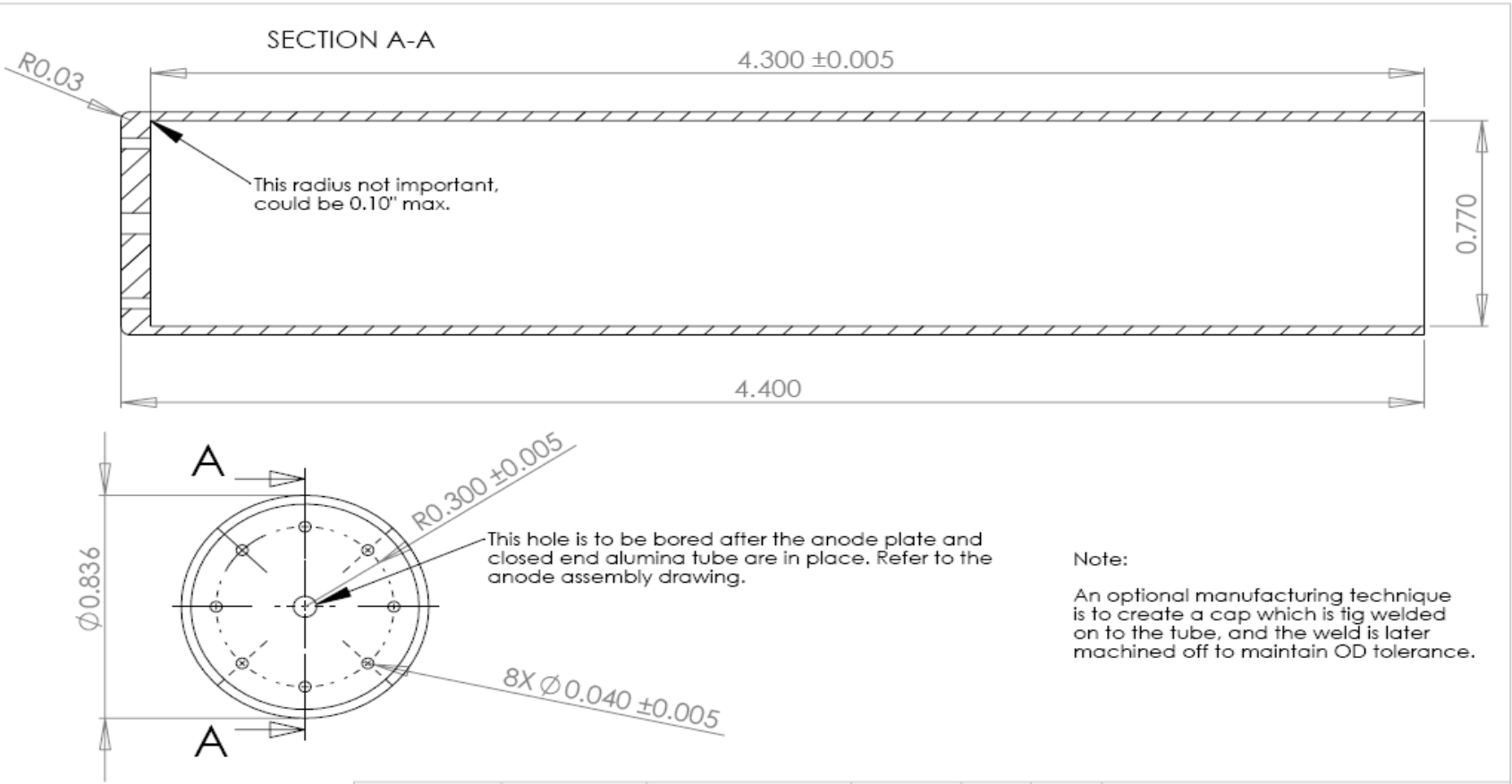

Note:

An optional manufacturing technique is to create a cap which is tig welded on to the tube, and the weld is later machined off to maintain OD tolerance.

		UNLESS OTHERWISE SPECIFIED:		NAME	DATE
		DIMENSIONS ARE IN INCHES TOLERANCES: TWO PLACE DECIMAL ±0.01 THREE PLACE DECIMAL ±0.001	DRAWN	JRC	07/21/06
			CHECKED		
			ENG APPR.		
			MFG APPR.		
		INTERPRET GEOMETRIC TOLERANCING PER:	Q.A.		
		MATERIAL 304 SS	COMMENTS: quantity : 2		
NEXT ASSY	USED ON	FINISH			
APPLICATION		DO NOT SCALE DRAWING			

TITLE: Anode Tube		
SIZE A	DWG. NO. Anode	REV 3
SCALE: 2:1	WEIGHT:	SHEET 1 OF 1

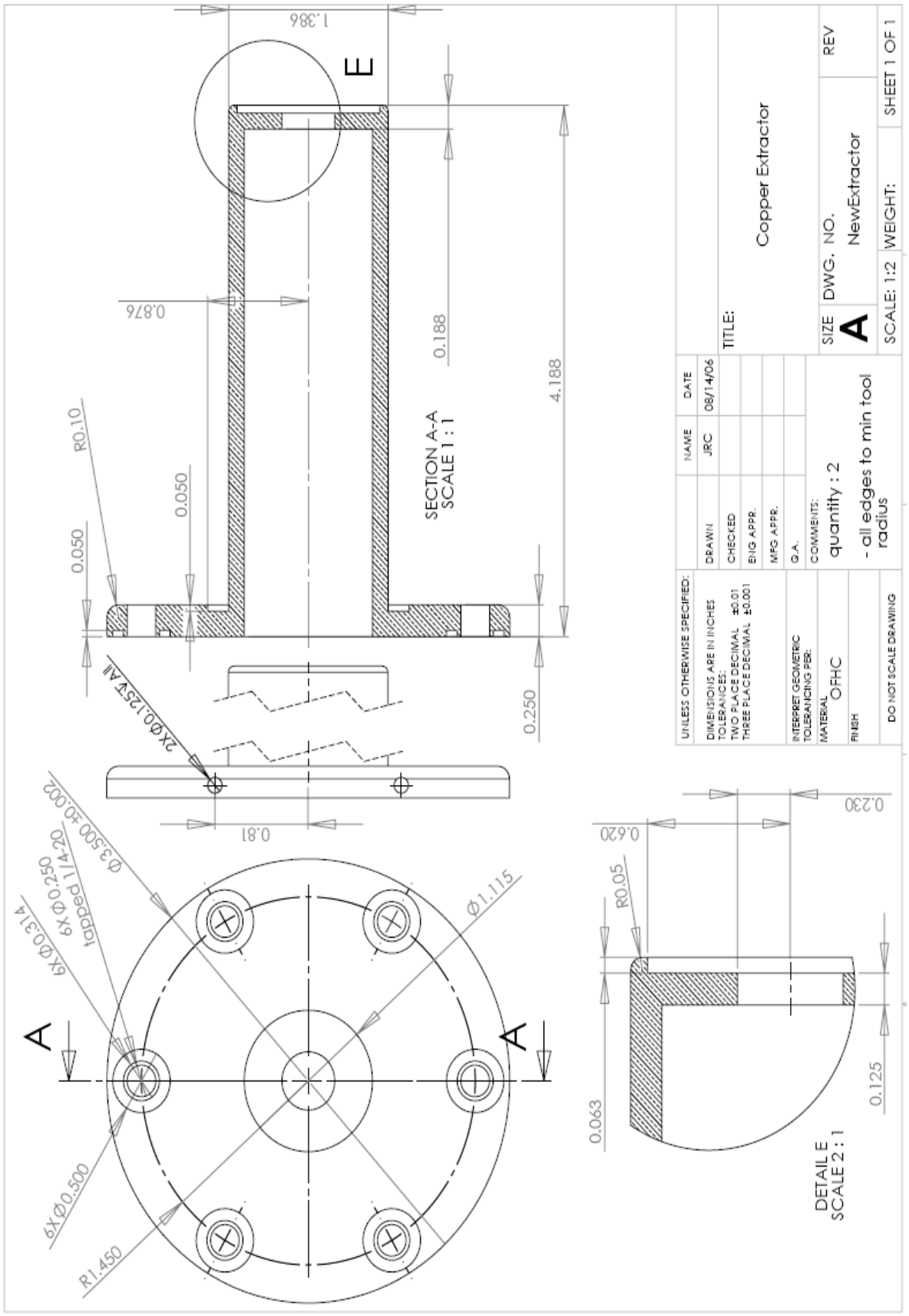
1.386
E
0.876
0.188
4.188
R0.10
0.050
0.050
SECTION A-A
SCALE 1 : 1
2X Ø0.125V A
0.250
0.81
Ø3.500±0.002
6X Ø0.314
tapped 1/4-20
6X Ø0.250
Ø1.115
A
A
6X Ø0.500
R1.450
0.230
0.620
R0.05
0.063
0.125
DETAIL E
SCALE 2 : 1
UNLESS OTHERWISE SPECIFIED:
DIMENSIONS ARE IN INCHES
TOLERANCES:
TWO PLACE DECIMAL ±0.01
THREE PLACE DECIMAL ±0.001
INTERPRET GEOMETRIC TOLERANCING PER:
MATERIAL
OFHC
FINISH
DO NOT SCALE DRAWING
NAME
DATE
DRAWN
JRC
08/14/06
CHECKED
ENG APPR.
MFG APPR.
G.A.
COMMENTS:
quantity : 2
- all edges to min tool radius
TITLE:
Copper Extractor
SIZE
A
DWG. NO.
NewExtractor
REV
SCALE: 1:2
WEIGHT:
SHEET 1 OF 1

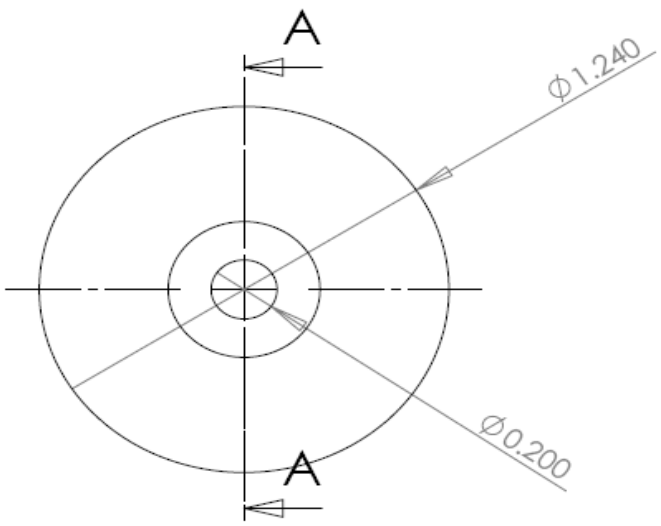

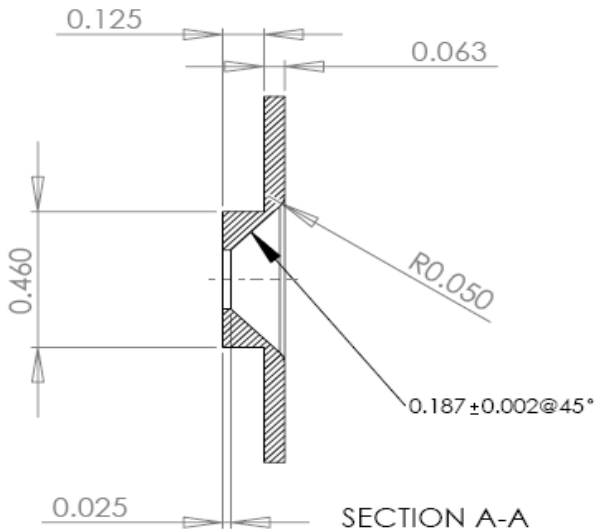

SECTION A-A
SCALE 2 : 1

UNLESS OTHERWISE SPECIFIED:		NAME	DATE
DIMENSIONS ARE IN INCHES TOLERANCES: TWO PLACE DECIMAL ±0.01 THREE PLACE DECIMAL ±0.001	DRAWN	JRC	08/14/06
	CHECKED		
	ENG APPR.		
	MFG APPR.		
INTERPRET GEOMETRIC TOLERANCING PER:	Q.A.		
MATERIAL Tantalum	COMMENTS: Quantity to be determined based on material availability (min 2), all edges to min tool radius.		
FINISH			
DO NOT SCALE DRAWING			

TITLE:
Tantalum Plate for Extractor

SIZE	DWG. NO.	REV
A	TantalumPlate	

SCALE: 1:1 | WEIGHT: | SHEET 1 OF 1

Appendix B: Vapor Pressure of the Elements

In Chapter 3 the vapor pressure of copper had to be taken into account when finding a suitable maximum temperature for the CFD simulations. The vapor pressure was found by using the following graph. Taken from Ref. (16).

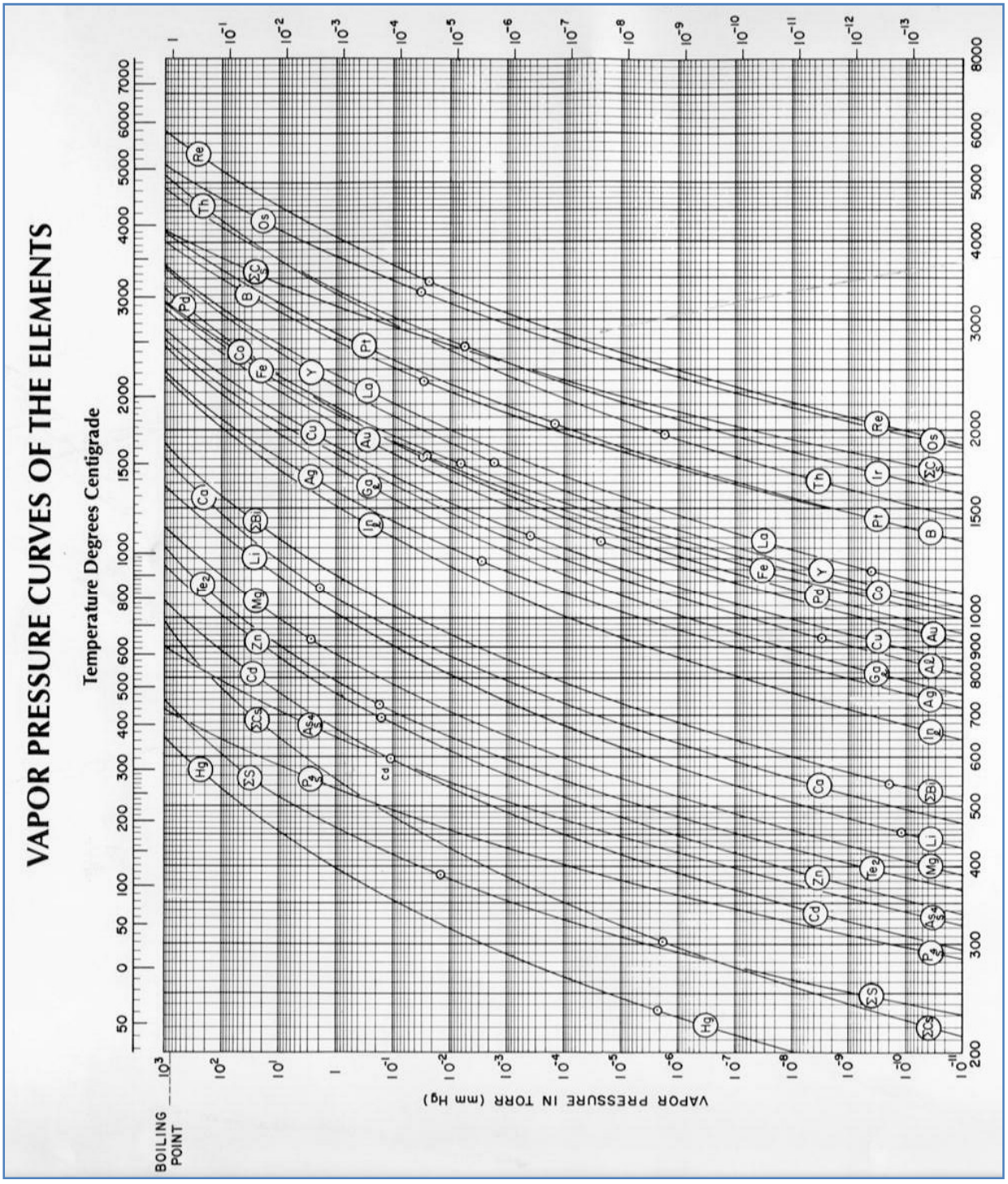

Appendix C: Emittance Calculation Code for Simion (PRG Code)

This code is the work of the author, and was used to calculate beam emittance in Simion (see Chapter 4). The PRG code is a user programming code unique to Simion. Particles were individually tracked to the point where they exited the simulation domain. At this point, the particles' velocities and positions were recorded in an array and manipulated to find the RMS emittance. The PRG code is not an efficient code to use but was previously the only available code for Simion. The latest release of Simion allows for the use of the Lua code, which makes user programs much faster (see Appendix D).

```
; This program will display the emittance of the beam at the ion splat location.
;
; The program is designed to monitor ions (mass > 1 amu), and ignore electrons
;
; Justin R. Carmichael 08/06/06

adefa Ysquared 2000             ; defining arrays large enough for all the particles
adefa Yprimesquared 2000
adefa Ytyprimesquared 2000
adefa y 2000
adefa yprime 2000
adefa velocityx 2000
adefa velocityy 2000


SEG Other_actions

        1
        RCL Ion_Mass            ; Here the program checks the ion mass, and if it
        X>=Y goto emittance     ; is an ion (amu larger than 1), it is counted.
        EXIT                    ; Move on if it isn't an ion.

LBL emittance                   ; start of data manipulation

        RCL Ion_Py_mm                   ; load the particles y position (in mm units)
        RCL ion_number                  ; load the particle's designated number
        asto y                  ; store in array 'y' (i.e. [ 1 , 1.234 mm ] )

        RCL Ion_Vx_mm                   ; find particle's x-velocity and store with number
        RCL ion_number                  ; in array 'velocityx'
        asto velocityx

        RCL Ion_Vy_mm                   ; same, but for velocity in 'y'
        RCL ion_number
        asto velocityy

        RCL Ion_Vy_mm                   ; load particle y-velocity in mm/s
```

```
        RCL Ion_Vx_mm               ; load particle x-velocity in mm/s
        Divide              ; do Vy / Vx
        Sto Yprime          ; store result as yprime

        RCL Yprime          ; load the yprime again
        RCL ion_number              ; load the associated ion number
        asto yprime         ; store result in yprime array

SEG Terminate

        1 sto n             ; let (n,c,g,p,u,w,m,r) = 1 (initially)
        1 sto c             ; these will be used in loops later on
        1 sto g
        1 sto p
        1 sto u
        1 sto w
        1 sto m
        1 sto r
        0 sto abc           ; these are initially 0, for loops as well
        0 sto cba
        0 sto pea
        0 sto ujk
        0 sto lpo

LBL step1

        rcl n               ; loop variable
        arcl y              ; get the value from array 'y' at 'n' location (intially 1)
        x=0 goto check      ; see comment at "LBL check"
        goto step2          ; move on

LBL step2

        sto lal             ; 'lal' and others like that are dummy variables
        rcl lal rcl lal *   ; do x^2 (y position squared)
        sto xsquared        ; store result as xsquared
        rcl xsquared        ; reload xsquared (if isn't already?)
        rcl n               ; reload 'n'
        asto Ysquared       ; store xsquared value at n space in myarray1
        rcl n 1 +
        sto n               ; do the n = n + 1 loop trick
        goto step1          ; back to the top...

LBL check

        ; this point is for checking the zero value in step1. normally a zero would correspond
        ; to a point where the array was empty, meaning there is no more data and to move on.
        ; However, the zero could -possibly- be a particle on the x axis, so this checks the
```

```
        ; array before moving on further...

        rcl n 1 +
        arcl y
        X=0 goto step3
        rcl n
        arcl y
        goto step2

LBL step3                       ; so we have y^2, now we want y'^2

        ; having a check for this section was considered unnecesary - the velocity shouldn't
        ; be zero in any beam...

        rcl c                   ; loop variable
        arcl yprime             ; get the value from array 'yprime' at 'c' location (intially 1)
        X=0 goto step4
        sto bas
        rcl bas rcl bas * ; do x^2 (y'^2)
        sto ypsquared           ; store result as ypsquared
        rcl ypsquared
        rcl c
        asto Yprimesquared
        rcl c 1 +       ; same loop trick for y-prime
        sto c
        goto step3

LBL step4                       ; here we do y times y-prime, loading both arrays

        rcl g
        arcl y
        sto why
        rcl g
        arcl yprime
        sto whyprime
        rcl why rcl whyprime *          ; y * y-prime
        sto multiple
        rcl multiple rcl multiple *     ; (y * y-prime) ^ 2
        sto multsq
        X=0 goto step5
        rcl multsq
        rcl g
        asto Ytyprimesquared            ; store result in this array...
        rcl g 1 +
        sto g
        goto step4                      ; loop back

LBL step5
```

```
        ; here the average of y^2 is found, and stored as 'ysave'

        rcl p
        arcl Ysquared
        sto one
        rcl p 1 +
        arcl Ysquared
        X=0 goto average5
        rcl one rcl abc +
        sto abc
        rcl p 1 +
        sto p
        goto step5

LBL average5                ; continuation of step 5, averaging

        rcl abc rcl p /
        sto ysave
        goto step6

LBL step6

        ; here the average of y-prime^2 is found

        rcl u
        arcl Yprimesquared
        sto var
        rcl u 1 +
        arcl Yprimesquared
        X=0 goto average6
        rcl var rcl cba +
        sto cba
        rcl u 1 +
        sto u
        goto step6

LBL average6

        rcl cba rcl u /
        sto ypsave          ; average (y-prime^2) = ypsave
        goto step7

LBL step7                   ; average for (y * y-prime)^2

        rcl w
        arcl Ytyprimesquared
        sto tea
```

```
        rcl w 1 +
        arcl Ytyprimesquared
        X=0 goto average7
        rcl tea rcl pea +
        sto pea
        rcl w 1 +
        sto w
        goto step7

LBL average7

        rcl pea rcl w /
        sto ytypsave            ; average (y * y-prime)^2 = ytypsave
        goto step8

LBL step8

        ; here the stored values are actually used to find the emittance
        ; (av[y^2]*av[y'^2]-av[(y*y')^2])^(1/2) , or:
        ; SQRT [ (ysave * ypsave) - ytypsave ]

        RCL ysave RCL ypsave *
        sto uno
        RCL uno RCL ytypsave -
        sto dos
        rcl dos abs
        sto dos
        rcl dos sqrt
        sto emittance
        goto finally

LBL finally

        ; here a message is generated to the user in the correct units

        1000
        RCL emittance *
        sto emitt
        rcl emitt
        MESS ; Beam Emittance = # mm * mrad
        goto velocity

        ; we also want to find the normalized beam emittance...

LBL velocity

        ; find the average velocity in the x-direction
```

```
        rcl m
        arcl velocityx
        sto gha
        rcl m 1 +
        arcl velocityx
        X=0 goto nextstep
        rcl gha rcl ujk +
        sto ujk
        rcl m 1 +
        sto m
        goto velocity

LBL nextstep

        RCL ujk rcl m /
        sto xavg                ; xavg = x-velocity average
        goto norm1

LBL norm1

        ; find the average velocity in the y-direction

        rcl r
        arcl velocityy
        sto klk
        rcl r 1 +
        arcl velocityy
        X=0 goto anotherstep
        rcl klk rcl lpo +
        sto lpo
        rcl r 1 +
        sto r
        goto norm1

LBL anotherstep

        RCL lpo rcl r /
        sto yavg                ; yavg = y-velocity average
        goto squared

LBL squared

        ; just SQRT [ V_x^2 + V_y^2 ]

        RCL xavg RCL xavg *
        sto xavgsq
        RCL yavg RCL yavg *
        sto yavgsq
```

```
        RCL xavgsq RCL yavgsq +
        sto plused
        RCL plused sqrt
        sto VelAvg              ; saved as VelAvg
        goto normalized

LBL normalized

        RCL VelAvg 300000 /     ; 300,000 = speed of light in mm/micro s
        sto BETA                ; result is stored as Beta
        RCL BETA RCL BETA *
        sto BETASQ
        1 RCL BETASQ -
        STO para
        RCL para SQRT
        sto nui                 ; nui = dummy variable
        RCL nui 1/X             ; this is gamma
        STO GAMMA
        RCL BETA RCL GAMMA * RCL emitt *
        sto NormBeam
        rcl NormBeam
        MESS ; Normalized Beam Emittance = # mm * mrad
```

Appendix D: Emittance Calculation Code for Simion (Lua Code)

The PRG code (Appendix C) was used by David Manura to create a more condensed and refined Lua program which is compatible with the latest release of Simion (version 8). His code is shown here.

```
-- emittance.lua
-- SIMION 8 user program to calculate emittance of beam at the splat location.
--
-- The program is designed to monitor ions (mass > 1 amu), and ignore electrons.
--
-- Author: Based on PRG code by Justin R. Carmichael 2006-08-06.
--         Converted to Lua by David Manura 2006-08-09.

-- various arrays to store variables on each particle
local y = {}       -- y positions (mm)
local yprime = {}  -- y' (radians)
local vx = {}      -- x-velocity (mm/usec)
local vy = {}      -- y-velocity (mm/usec)

-- Compute y-emittance from points in phase space.
-- parameters:
--   y - array of y points (mm)
--   yprime - array of angles (radians)
--   vx - array of x-velocities
--   vy - array of y-relocities
-- returns
--   emit - emittance
--   norm_emit - normalized emittance
function compute_emittance(y, yprime, vx, vy)
  local particle_count = #y  -- number of particles recorded

  -- compute various averages for emittance
  local y2_sum = 0
  local yprime2_sum = 0
  local yyprime_sum = 0
  for n = 1,particle_count do
    y2_sum      = y2_sum      + y[n]^2
    yprime2_sum  = yprime2_sum + yprime[n]^2
    yyprime_sum  = yyprime_sum + (y[n] * yprime[n])
  end
  local y2_ave = y2_sum / particle_count
  local yprime2_ave = yprime2_sum / particle_count
  local yyprime_ave = yyprime_sum / particle_count

  -- compute emittance from averages, in correct units
  local emit = sqrt(y2_ave * yprime2_ave - yyprime_ave^2) * 1000
```

```
  -- compute average speed for normalized emittance
  local vx_sum = 0
  local vy_sum = 0
  --FIX: or this: local v_sum = 0
  for n = 1,particle_count do
    vx_sum = vx_sum + vx[n]
    vy_sum = vy_sum + vy[n]
    --FIX: or this: v_sum = v_sum + sqrt(vx[n]^2 + vy[n]^2)
  end
  local vx_avg = vx_sum / particle_count
  local vy_avg = vy_sum / particle_count
  local v_avg = sqrt(vx_avg^2 + vy_avg^2)
  --FIX: or this: local v_avg = v_sum / particle_count

  -- compute normalized emittance from averages
  local c = 300000                -- speed of light (mm/usec)
  local beta = v_avg / c          -- relativistic beta
  local gamma = 1 / sqrt(1 - beta^2)  -- relativistic gamma
  local norm_emit = beta * gamma * emit

  return emit, norm_emit
end

-- SIMION segment called on every time-step
function other_actions()
  if ion_mass < 1   then return end -- skip if not any ion (amu < 1)
  if ion_splat == 0 then return end -- skip if ion not yet splatted.

  -- store variables for emittance calculation
  local particle_count = #y + 1
  y[particle_count] = ion_py_mm    -- store y position (mm)
  vx[particle_count] = ion_vx_mm   -- store x-velocity (mm/usec)
  vy[particle_count] = ion_vy_mm   -- store y-velocity (mm/usec)
  yprime[particle_count] = ion_vy_mm / ion_vx_mm  -- store ~tan(theta)
  -- FIX? or this: yprime[particle_count] = atan2(ion_vy_mm, ion_vx_mm)
end

-- SIMION segment called on every particle termination.
function terminate()
  if ion_number ~= 1 then return end -- only do this once

  -- calculate/display emittance
  local emit, norm_emit = compute_emittance(y, yprime, vx, vy)
  print("Beam Emittance = " .. emit .. " mm * mrad (Normalized = " .. norm_emit .. ")")
end
```

Bibliography

1. **Stair, Billy.** Oak Ridge National Laboratory Fact Sheet. [Online] 2007. [Cited: November 10, 2007.] http://www.ornl.gov/ornlhome/fact.pdf.

2. *Sprinting into the New Millenium: The Latest Chapter in ORNL History (1993-2003).* **ORNL.** 2003, ORNL Review, pp. 25-34.

3. *Returning Home.* **ORNL.** 2006, ORNL Review, pp. 2-3.

4. *That's Incredible - Some amazing facts about the Spallation Neutron Source.* **ORNL.** 2006, ORNL Review, p. 7.

5. **Webster, John A.** Los Alamos National Laboratory Daily NEWSBulletin. [Online] October 26, 1998. [Cited: November 23, 2007.] http://www.lanl.gov/orgs/pa/News/102698.html.

6. **Lieberman, Michael A. and Lichtenburg, Allan J.** *Principles of Plasma Discharges and Materials Processing.* Hoboken : John Wiley & Sons, Inc., 2005.

7. *Design, Operational Experiences and Beam Results Obtained with the SNS H- Ion Source and LEBT at Berkeley Lab.* **Keller, R., et al.** 2002, 9th International Symposium on the Production and Neutralization of Negative Ions and Beams, pp. 1-13.

8. **Welton, Robert F.** *A Helicon Ion Source for the SNS Power Upgrade.* Oak Ridge : LDRD FY 2007, 2006. Presentation.

9. **Dr. Robert F. Welton.** Oak Ridge National Laboratories, SNS Ion Source Physicist (personal communication).

10. *Longitudinal magnetic field effect on the electrical breakdown in low pressure gases.* **Petraconi, G., et al.** 4b, São Paulo : Brazilian Journal of Physics, 2004, Vol. 34. 0103-9733.

11. *Characteristics of the Hollow Anode Ion-Electron Source.* **Miljevic, V.I.** 5, s.l. : IEEE Transactions on Nuclear Science, 1985, Vol. 32.

12. *Hollow anode ion source.* **Miljevic, V.I.** 1, s.l. : Rev. Sci. Instrum., 1990, Vol. 61.

13. **Case Technology, Inc.** Ion Source Technology. [Online] September 14, 2005. [Cited: February 10, 2008.] http://www.casetechnology.com/source.html.

14. **Mahaney, Shawn; Kim, Dr. Chung-Whee;.** Modeling of the Die Cast Process - A Finite Element Method Approach. *EKK, Inc.* [Online] 2002. [Cited: January 18, 2008.] http://www.ekkinc.com/nvgartcl.htm.

15. **COSMOS.** COSMOSFloWorks - CFD (Computational Fluid Dynamics) for Flow Analysis and Simulation. *SolidWorks.* [Online] 2008. [Cited: January 18, 2008.] http://www.solidworks.com/pages/products/cosmos/cosmosfloworks.html.

16. **McAllister Technical Services.** A Short History of Vacuum Terminology and Technology. *McAllister Technical Services.* [Online] May 13, 2001. [Cited: January 18, 2008.] http://www.mcallister.com/vacuum.html.

17. **Goodfellow.** Alumina - Material Information. *Goodfellow.* [Online] [Cited: January 18, 2008.] http://www.goodfellow.com/csp/active/static/E/Alumina.HTML.

18. **COSMOS.** COSMOSWorks. *SolidWorks.* [Online] 2008. [Cited: January 27, 2008.] http://www.solidworks.com/pages/products/cosmos/cosmosworks.html.

19. **Engineer's Edge.** Strength of Materials - Mechanics of Materials. *Engineer's Edge.* [Online] 2008. [Cited: January 26, 2008.] http://www.engineersedge.com/strength_of_materials.htm.

20. **Hibbeler, R. C.** *Mechanics of Materials.* Upper Saddle River : Pearson Prentice Hall, 2008. 0-13-220991-8.

21. **PBGUNS.** J.E. Boers. Thunderbird Simulations, 626 Bradfield Dr. Garland, Texas 75042.

22. **Keller, R.** Ion Extraction. [book auth.] Ian G. Brown. *The Physics And Technology Of Ion Sources.* New York : John Wiley & Sons, Inc., 1989.

23. **Simion 8.0.** available through Scientific Intrument Services Inc., 1027 Old York Rd., Ringoes, NJ 08551.

24. **D.J. Manura.** Scientific Instrument Services Inc., personal communication.